Construction and Building Materials 547 (2026) 148592

Contents lists available at ScienceDirect

Construction and Building Materials

journal homepage: www.elsevier.com/locate/conbuildmat

From paste to concrete: Dosage-dependent non-linear flow behavior and superplasticizer demand governed by calcined clay type

Axel Neißer-Deiters *, Sebastian Scherb, Nancy Beuntner, Karl-Christian Thienel

Civil Engineering and Environmental Science, Bundeswehr University Munich, Werner-Heisenberg-Weg 39, Neubiberg, 85579, Germany

ARTICLE INFO

Keywords:
2:1 phyllosilicate
Illite
Smectite
Thixotropy
Shear thickening
Workability retention
Rheology

ABSTRACT

Calcined clays are promising supplementary cementitious materials, but can impair initial flowability and workability retention in concrete. This study investigated the influence of five superplasticizers on the early flow behavior of 70/30 vol% cement/calcined clay systems with four calcined 2:1 phyllosilicates with different illite and smectite contents. Over 2 h, rotational rheometry was applied to paste and concrete, and spread-flow tests to paste, mortar, and concrete, focusing on non-linear flow behavior and thixotropy. Across paste, mortar, and concrete, superplasticizer demand was governed by calcined clay type rather than superplasticizer type. The general demand followed the order illite > smectite/illite mixture > smectite, although the ranking changed slightly in concrete and quantitative prediction from paste to concrete was not possible. Diverging rheological impacts of seemingly similar clays may stem from colloidal interactions. Workability-retention challenges appeared to originate in the initial flow state: the flowability improvement from superplasticizers decreased by more than 60% within 2 h. A systematic dosage study for one calcined illite in paste showed that a flocculation-based thixotropic recovery became increasingly dominant at higher dosages, in addition to a suggested dosage-independent platelet-based contribution, whereas shear thickening increased with dosage and was confirmed across all investigated calcined clays. A moderate dosage provided the best workability retention. In concrete, limited data indicated pronounced static yield stress, shear-history dependence, and apparent saturation limits for certain clay–superplasticizer combinations. Overall, high superplasticizer dosages in calcined clay systems may impair workability retention or induce shear thickening, shifting the optimum toward lower dosages.

1. Introduction

Calcined clays are promising supplementary cementitious materials for reducing the clinker content and carbon footprint of concrete due to their broad availability and pozzolanic reactivity after calcination [1]. While kaolinite-rich calcined clays have been studied extensively [2], many natural clay deposits also contain substantial amounts of 2:1 phyllosilicates such as illite and smectite [3–5]. These clays are relevant for expanding the raw material basis for potential calcined clays, but their use remains challenging as they can strongly affect fresh-state behavior, superplasticizer (SP) demand, and workability retention [6,7].

1.1. Time- and shear-history-dependent rheological behavior

Thixotropy describes a reversible, time-dependent phenomenon in which the resistance to flow of a material decreases over time while a constant shear rate is applied, and recovers when the material is subsequently left at rest [8]. Thixotropy is generally attributed to an interparticle network that forms at rest and is governed by attractive interactions between particle surfaces. When shear is applied, this network (sometimes named interparticle bridges) is destroyed, resulting in a lower shear stress response [8]. The initial break up of interparticle forces is related to the term static yield stress [9].

In cementitious systems, the short interparticle distances favor van der Waals attraction and flocculation [10,11], and ongoing hydration continuously changes surfaces, pore solution, and adsorption, so that the rheological response depends on both time and shear history [9].

Experimentally, thixotropy is closely linked with structural breakdown. While thixotropy is reversible, structural breakdown describes an irreversible decrease in the shear stress response, commonly attributed to the rupture of bonds that do not reform, such as early hydrate bridges between particles [12,13]. Hysteresis loops are commonly used to assess

* Corresponding author.
E-mail addresses: axel.neisser-deiters@unibw.de (A. Neißer-Deiters), sebastian.scherb@unibw.de (S. Scherb), nancy.beuntner@unibw.de (N. Beuntner), christian.thienel@unibw.de (K.-C. Thienel).

https://doi.org/10.1016/j.conbuildmat.2026.148592
Received 10 August 2026; Received in revised form 14 October 2026; Accepted 15 October 2026
Available online 22 October 2026
0950-0618/© 2026 The Author(s). Published by Elsevier Ltd. This is an open access article under the CC BY license (http://creativecommons.org/licenses/by/4.0/).
Open access funding enabled and organized by Projekt DEAL.

time-dependent behavior, but they cannot clearly distinguish between reversible thixotropy, irreversible structural breakdown, and hydration-related structuration [8]. Step profiles are therefore useful, because the recovery of stress or viscosity after a sudden decrease in shear rate provides an additional indication of thixotropic behavior [14].

1.2. Effect of calcined clays

Calcined clays can strongly affect the fresh-state behavior of cementitious systems. Their high specific surface area (5–95 m^2/g) [5,7,15], platelet-like particle morphology [16,17], water adsorption capacity [18–21], and surface charge [22,23] increase the number and strength of particle interactions and can therefore increase yield stress, thixotropy [24], and SP demand [20]. In addition, calcined clays can accelerate early hydration [15,25], including ettringite formation [26], which may further contribute to structural build-up [21] and workability loss [27].

The rheological impact of calcined clays depends strongly on clay mineralogy and cannot be inferred from a single material parameter alone. Differences in surface charge, water adsorption, swelling behavior, particle morphology, and SP interaction can lead to substantially different fresh-state responses even for calcined clays with comparable surface area or clay content [17,28–30]. Consequently, their rheological behavior should be evaluated with regard to clay mineralogy and subsequent parameters rather than treating calcined clays as a uniform material class. Shear-dependent flow behavior can also vary in calcined clay systems. Reported trends are not uniform, with near-Bingham, shear-thinning, and shear-thickening behavior all being described for cementitious systems containing calcined clays [6,17,29,31–33]. Whether such non-linearity is captured depends on the applied model, since fitting a Bingham model to a shear-thickening material can return a physically meaningless negative yield stress [34]. This is addressed by the quadratic and power-law extensions such as the modified Bingham and Herschel–Bulkley models [35–37]. A comparison of models is therefore required before shear-dependent behavior can be interpreted [38]. Calcined clays can also increase static yield stress and thixotropy, with reported increases linked to negative surface charge, high water demand, and changes in early hydration products [23,39,40].

Within the group of 2:1 phyllosilicates, illitic and smectitic calcined clays affect superplasticizer demand differently. A calcined smectitic clay required about one third the superplasticizer than a calcined kaolinitic clay to reach comparable mortar flow [41], whereas calcined illites and muscovites reduced superplasticizer efficiency compared with metakaolin [42]. At a fixed superplasticizer dosage, pastes containing metamuscovite showed shear thickening, which was not observed for metakaolin [42]. Flow loss in the presence of superplasticizer has been attributed to newly formed hydrate surfaces that are not covered by superplasticizer, for calcined montmorillonite as well as for kaolinitic clays [43]. In cement-free solutions, calcined smectitic clays showed no swelling, and superplasticizer adsorption was low in comparison to calcined illitic clays [30].

1.3. Role of superplasticizers

Polycarboxylate ether (PCE) SPs improve dispersion by increasing electrostatic and steric repulsion between particles, thereby increasing particle separation and reducing attractive interparticle forces. As a result, higher SP adsorption and surface coverage have been associated with lower static yield stress and reduced thixotropic structural build-up [24,44,45].

However, this effect is not universal, since the molecular structure of the PCE and its influence on early hydration can also affect thixotropy. In particular, shorter side-chains or a higher anionic charge density have been reported to alter early hydrate formation and thereby increase thixotropic structural build-up [46,47]. Thus, SPs influence fresh-state behavior not only through initial dispersion, but also through adsorption, surface coverage, molecular structure, and hydration-related changes during the first hours after mixing.

1.4. Research gap and scope of this study

Paste and mortar measurements are often used to study binder-related rheological effects because concrete rheometer measurements require substantially more material, labor, and time. For conventional ordinary Portland cement-based systems, Wallevik [48] reported that mortar and concrete yield values correlate strongly, whereas the corresponding relationship for plastic viscosity was weak, partly due to effects such as plug flow, air entrainment, and gravel migration. This indicates that paste-level or mortar-level measurements can provide useful tendencies, but that transferability depends on the rheological parameter considered [49]. For calcined clay systems, this transferability must be evaluated separately, because aggregate packing, paste film thickness, particle mobility, and calcined clay–SP interactions may further modify the concrete response. To the authors' knowledge, the influence of 2:1 phyllosilicate dominated calcined clay type on SP demand and workability retention has not been assessed consistently across paste, mortar, and concrete, and the effect of SP dosage on transient and non-linear flow behavior beyond the initial flowability has not been systematically examined for such systems.

This study investigates the influence of 2:1 phyllosilicate dominated calcined clay types, SP type, and SP dosage on the early flow behavior of 70/30 vol% OPC/calcined clay systems. Four calcined clays with different illitic and smectitic contents are evaluated in paste, mortar, and concrete. SP demand and workability retention are assessed by spread-flow measurements, while rotational wide-gap rheometry is applied to paste and, for selected flowable mixtures, to concrete in order to evaluate yield stress, viscosity, flow resistance, thixotropy, structural breakdown, and shear-dependent flow behavior. Particular attention is paid to whether paste and mortar results indicate concrete behavior and how higher SP dosages affect rheological behavior beyond the commonly evaluated initial flowability. The calcined clays and one of the SPs studied here were previously characterized in cement-free clay–SP suspensions [30]; the present study adds the cementitious matrix, the SP dosage variation, and the transfer to paste and concrete.

2. Materials and methods

2.1. Materials

2.1.1. Binder materials

An ordinary Portland cement CEM I 42.5 N (OPC) was used in all mixtures. The OPC had a water demand of 27 wt% [50], a spread flow of 166 mm [51], a density of 3.12 g/cm^3 [52], and a Blaine specific surface area of 2740 cm^2/g [53]. The particle size distribution was characterized by d_{10}, d_{50}, and d_{90} values of 4.2, 23.4, and 63.1 μm [54], respectively. The mineralogical composition of the cement, as provided by the supplier, is given in Table 1.

Four 2:1 phyllosilicate dominated clays were used in this study. The methods and results of the mineralogical (Table 2), chemical, and physical (Table 3) characterization, as well as the calcination and grinding conditions, are described in full in [30]. The data relevant to the present work are repeated here for the reader's convenience; the complete mineralogical composition is given in the supplementary material (Table S1).

Zeta potential was determined via electro acoustic measurement using a DT-310 spectrometer Dispersion Technology Inc (Table 4). The liquid/solid ratio used was 3.0. Given values are based on the average of six measurements. Temperature was 23 °C. Solutions used were deionized water (DIW), a 0.12 M KOH solution (KOHS), and synthetic cement pore solution (SCPS) according to [59].

Table 1
Mineralogical composition of OPC in cement chemistry notation. The producer is not named for confidentiality reasons.

	C_3S	C_2S	C_3A	C_4AF	M	C	$C\bar{S}$	$C\bar{S}H_{0.5}$	$C\bar{S}H_2$	$C\bar{C}$	Other phases
OPC [wt%]	60.4	18.2	6.5	8.3	0.9	0.4	1.5	0.7	0.2	0.8	2.1

Table 2
Mineralogy of raw clays; feldspar, carbonates, quartz, and constituents of less than 5 wt% are summed up in the last column. The complete mineralogical composition is given in the supplementary material. Data from [30].

[wt%]	kaolinite	illite / mica	smectite	other constituents
rIIIE	10	74		16
rIIIA	7	72		21
rSmk	7	4	54	35
rSmI	11	33	33	23

2.1.2. Superplasticizers

Three polyethylene glycol type SPs were synthesized from polyethylene glycol methallyl ether side-chain (often referred to as HPEG) and acrylic acid backbone monomers. The SPs were named according to the side-chain length, expressed as the number of ethylene oxide units, and the molar ratio of backbone monomer (a) to side-chain macromonomer (b).

The SP 52HPEG6 was previously used in [30], while two additional lab synthesized SPs are included in the present study (Table 5). These three SPs were synthesized and characterized by a joint research partner at the Technical University of Munich.

Additionally, two industrial PCE were included in the study. One industrial PCE was designed for common ready-mix concrete (RM-SP), intended for high initial flowability and slump retention. The second industrial PCE was specifically designed for a slump-retaining mix (SR-SP) in a system with calcined clays, with moderate initial flowability. No further characteristics of the two industrial PCEs were disclosed by the supplier. All SP dosages in this study refer to the solid content and are given by weight of binder (%bwob).

2.2. Mixture design and mixing procedure

2.2.1. Mixture design

Boundaries for mixture design are displayed in Table 6. The binder mass was kept constant for each medium, whereas the cement-to-calcined-clay ratio was proportioned volumetrically. Because the calcined clays differ slightly in particle density (Table 3), the binder volume and thus the total density of the mixtures vary marginally. Since the aggregate mass was also kept constant, the aggregate volume fractions given for mortar and concrete are design values; the resulting deviation between mixtures is below 0.1 vol%. CEN standard sand was used as aggregate for mortar [51], whereas a natural limestone aggregate was used for concrete. Liquid content of SPs was deducted from water addition. Throughout this paper, cIIIE, cIIIA, cSmk, and cSmI denote the calcined clays; the corresponding suspensions are referred to as, e.g., cIIIE paste, cIIIE mortar, and cIIIE concrete.

Table 4
Zeta potential measurements and pH data in three solutions.

Calcined clay	DIW		KOHS		SCPS	
	pH	Zeta potential	pH	Zeta potential	pH	Zeta potential
	[-]	[mV]	[-]	[mV]	[-]	[mV]
cIIIE	7.7	-34.9	12.8	-34.8	12.9	-11.2
cIIIA	11.1	-17.8	12.9	-20.7	13.0	-7.5
cSmk	9.9	-18.2	12.9	-19.4	13.0	6.2
cSmI	5.9	-19.6	12.8	-17.9	12.8	6.4

2.2.2. Mixing protocol

The mixing protocol is displayed in Fig. 1. Paste and mortar mixing protocols are generally according to the relevant normative regulations [50,51]; including the prescribed rotary/planetary speeds of 140/62 rpm at low speed and 285/125 rpm at high speed. The exceptions were an initial dry-mixing when different binder solids were used and an initial hand mixing after water addition to ensure all solids are scraped off the wall and are within the range of the paddle. The concrete mixing was done with a mixer UEZ LZ 35/50 from UEZ Mischtechnik GmbH with 48 rpm.

2.3. Rheometric measurements and data evaluation

2.3.1. Rheometer setup and measurement procedure

Rheometric measurements were performed using rotational wide-gap rheometers. Paste was measured with a Viskomat NT, while concrete was measured with a Viskomat XL. Both devices were manufactured by Schleibinger Geräte Teubert und Greim GmbH. Since both instruments are wide-gap rheometers, the determined rheological parameters are rheometer-specific and should therefore be interpreted as apparent values. For the Viskomat NT, the measuring system used a cup with an inner diameter of 83 mm, a filling height of 70 mm, and a bottom clearance of 2 mm. Paste was measured with a window paddle of 61 mm height. For the Viskomat XL, concrete was measured in a cup with an inner diameter of 165 mm and an inner depth of 165 mm, using a vane paddle with a diameter of 69 mm and a height of 69 mm, resulting in a radial gap of 48 mm and a bottom clearance of 48 mm, as described in [9,61].

Water and solid materials were stored at approximately 25 °C prior to testing. The sample was poured into the rheometer cup approximately 6 min after water addition, using a sample volume of 370 ml for the Viskomat NT and 3000 ml for the Viskomat XL, corresponding to a filling height of 70 mm and 140 mm, respectively. The rheometer cup was equipped with a water-cooling unit set to 25 °C. The rheometer

Table 3
Physical parameters of the calcined clays used, data from [30].

Parameter	Test method			cIIIE	cIIIA	cSmk	cSmI
particle density	[52]		[g/cm³]	2.76	2.72	2.72	2.82
BET specific surface area	[55]		[m²/g]	70.6	67.2	37.9	50.9
particle size distribution	[54]	d_{10}	[µm]	2.8	2.5	2.4	2.6
		d_{50}	[µm]	15.8	15.8	15.8	15.6
		d_{90}	[µm]	49.6	60.7	56.3	60.5
water demand	[56]		[wt%]	53.4	55.6	45.0	50.6
water adsorption capacity	[57]		[wt%]	65.4	75.3	50.3	66.1
cation exchange capacity	[58]		[cmol(+)/kg]	11	12	7	7

Table 5
SPs characteristics provided by the joint research partner. Data for 52HPEG6 are taken from [30]. Molecular weights are M_n and M_w; PDI is the polydispersity index. Detailed information on methodology for SP characterization can be found in [60].

PCE samples	a:b	side-chain	M_w	M_n	PDI	Conversion rate of macromonomer	Measured anionic charge amount
	[-]	[n_{EO}]	[g/mol]	[g/mol]	[M_w/M_n]	[%]	[µeq/g]
23HPEG10	10	23	16530	9959	1.7	99.0	6040
52HPEG6	6	52	14940	10550	1.4	93.4	2146
52HPEG10	10	52	23570	16060	1.5	98.8	3745

Table 6
Boundaries for mixture design. Grading curves of aggregates can be found in the supplementary material (Figure S1).

	paste	mortar	concrete
Aggregate size	-	0–2 mm	0–8 mm
Aggregate density	-	2.65 kg/dm³	2.73 kg/dm³
Aggregate volume (design)	-	70 vol%	66 vol%
Gravimetric water binder ratio	0.5	0.5	0.5
CEM/CC	70/30 vol%	70/30 vol%	70/30 vol%

profile was started 10 min after water addition. The data sampling rate was set to 10 Hz, corresponding to approximately 9.92 Hz in the exported Excel files.

Each calcined clay paste–SP combination was measured on at least two separately mixed batches. Replicates were considered reproducible if the transient and shear-dependent torque response agreed in shape; a parallel offset in torque level was tolerated as long as the residual pattern of the model fits (Section 2.3.4) remained unchanged. For this assessment, each batch was fitted separately and accepted if the residuals showed the same sign pattern and comparable magnitude over the covered speed range; otherwise a third batch was measured. One representative measurement was then used for further evaluation to avoid altering the original flow behavior by averaging data points. Data processing was performed in RStudio 2026.04.0. The evaluation script was written by the authors with AI-assisted code support (OpenAI ChatGPT, various model versions between 2023 and 2026). Evaluation was based on raw data unless smoothing was explicitly stated. Where smoothing was applied, a 30-point forward moving average was used unless stated otherwise. Graphical analysis was carried out in OriginLab 2023.

The rheometer profile for paste is shown in Fig. 2 bottom, and the profile for concrete is displayed in Fig. 2 top. Both profiles followed the same general sequence, consisting of a pre-shear phase (0–45 s) and a rest phase (45–180 s), followed by a ramp-up, a short holding period at maximum rotational speed, and a ramp-down (Ramp1, 180–300 s). This was followed by stepwise decreases from the maximum rotational speed (steps, 305–620 s), in 10 rpm steps for the Viskomat NT with a maximum of 100 rpm and in 1 rpm steps for the Viskomat XL with a maximum of 8 rpm, except for the last two steps, which were reduced by 0.5 rpm and 0.3 rpm, with each step lasting 30 s and including a step transition of 1 s. After the step profile, the pre-shear (620–671 s), rest (671–806 s), ramp-up, and ramp-down sequence was repeated in mirrored form (Ramp2, 806–926 s) until the end of the test. These phase designations and time intervals are used consistently in the following sections. For better visibility, the step analysis is displayed only for selected steps in Fig. 2.

2.3.2. Integral-based evaluation of ramp sections

For rheological evaluation, several parameters were calculated from the torque response. Four ramp integrals were determined from ramp1up, ramp1down, ramp2up, and ramp2down, as indicated in Fig. 2 in pink. The area under each shear ramp was calculated by numerical integration of torque over rotational speed using the composite trapezoidal rule. For decreasing ramps, the absolute value of the integral was used to obtain positive area values. The integration boundaries were: Viskomat NT: 0.5 rpm < integration range < 99.95 rpm; Viskomat XL: 0.1 rpm < integration range < 7.95 rpm. The integral of ramp1down was considered as the flow resistance parameter originally introduced by [62]. At each step the first 25 s were used to calculate the transition integral (Fig. 2, brown) and last 5 s to calculate the equilibrium integral (Fig. 2, green).

The ramp integrals were further used to calculate hysteresis and structural breakdown parameters. Hyst1 and Hyst2 were calculated from the hysteresis loops of Ramp1 and Ramp2, respectively (Eq. 1 and Eq. 2). Hyst-values close to 1 indicate that neither thixotropy nor structural breakdown is dominant. Hyst-values different from 1 indicate thixotropic behavior and/or structural build-up or breakdown. The structural breakdown factor (SBF) describes the change in the Ramp2 integrals compared with Ramp1 (Eq. 3).

$$Hyst1 = \frac{integral\ ramp1down}{integral\ ramp1up} \tag{1}$$

$$Hyst2 = \frac{integral\ ramp2down}{integral\ ramp2up} \tag{2}$$

$$SBF = \frac{integral\ ramp2down + integral\ ramp2up}{integral\ ramp1down + integral\ ramp1up} \tag{3}$$

2.3.3. Step-based evaluation and equilibrium criteria

For each step, the torque signal was integrated over the first 25 s after the step change (transition integral) and over the final 5 s of the step (equilibrium integral). Both integrals were divided by their respective time intervals to obtain time-normalized average torque values. The transient factor was then calculated as the relative difference between the average torque during the initial transition period and the average torque during the final equilibrium period (Eq. 4).

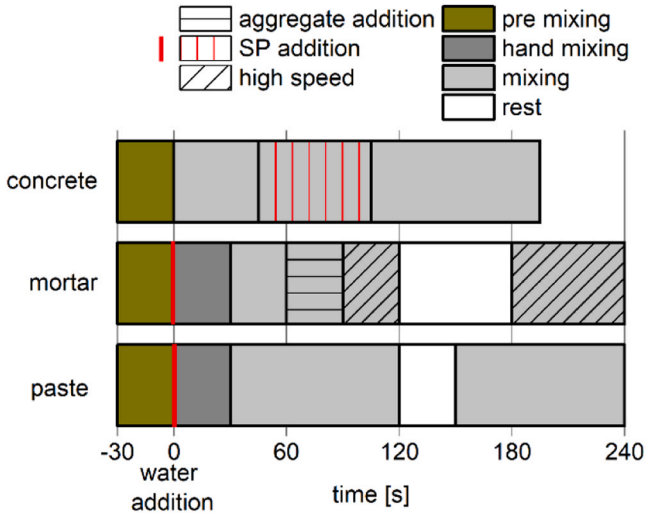


Fig. 1. Mixing protocols for the media tested. Paste mixing protocol is according to [50]; mortar is according to [51].

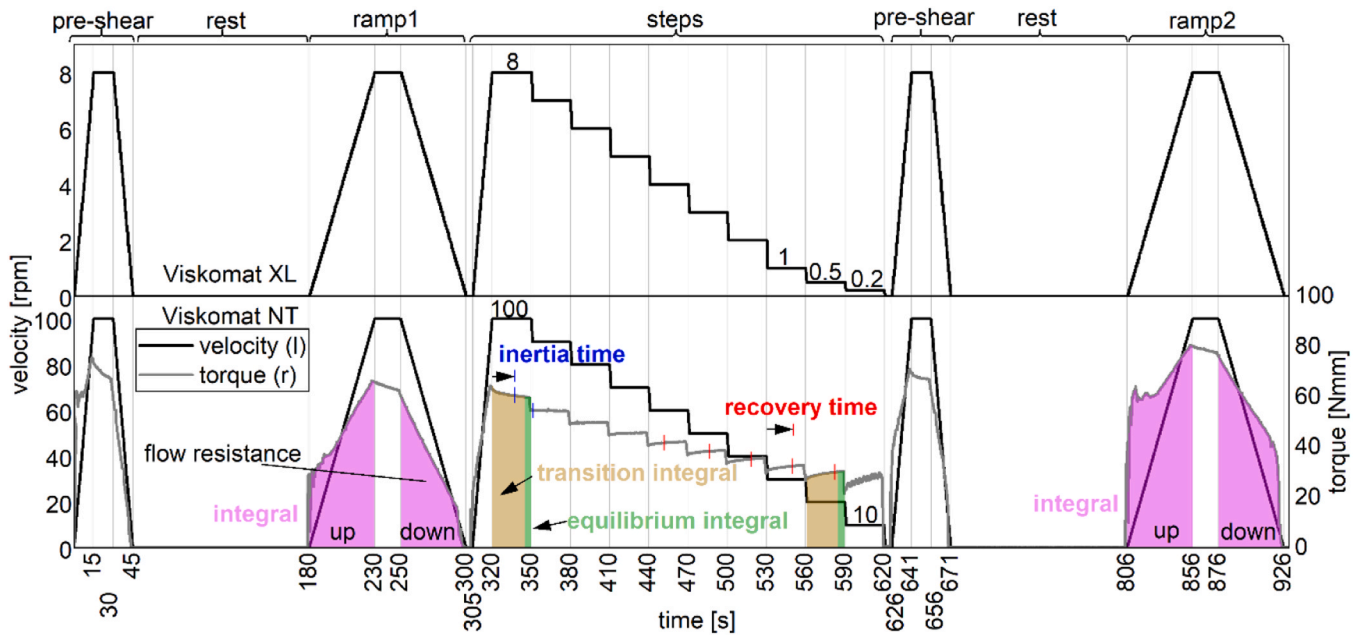


Fig. 2. Rheometer program for Viskomat NT (bottom) and Viskomat XL (top). Step analysis was done on every step for NT and XL, but for better visibility it is only displayed in this figure on NT steps 100 and 20 rpm. For the Viskomat NT, an exemplary torque profile is shown for visualizing the analysis of the torque values.

$$transientfactor = (1 - \frac{transition\ integral/25\ \ s}{equilibrium\ integral/5\ \ s}) * 100 \quad (4)$$

The equilibrium integral was also used to calculate the equilibrium mean torque. With a sampling rate of approximately 9.92 Hz, the final 5 s corresponded to approximately 49 data points. Equilibrium mean torque values were only used for flow model calculations if equilibrium was reached during the final 5 s of the respective step. Equilibrium was defined by a torque slope below 0.05 Nmm/s and a coefficient of variation below 1%.

Transition time was separated into inertia time and recovery time, depending on the direction of the torque response after a step change. Both parameters describe the time required for the torque response to reach a range of ±1% around the mean torque value of the new step. If the torque response decreased towards the equilibrium value after the step change, this period was defined as inertia time and is shown in Fig. 2 in blue. If the torque response initially overshot and subsequently increased or recovered towards the equilibrium value, this period was defined as recovery time and is shown in Fig. 2 in red.

Due to technical limitations, the Viskomat NT showed higher deviations at 10 rpm. Therefore, the 10 rpm data were excluded from rheological analysis.

2.3.4. Rheological model fitting

Rheological parameters were calculated from equilibrium points obtained during the step profile. Unless stated otherwise, yield stress refers to the dynamic yield stress.

The Bingham model (Eq. 5) was used as the default model for all datasets that fulfilled the equilibrium criteria. To assess whether non-linear flow behavior had to be considered, a modified Bingham model (Eq. 6) was additionally evaluated, and the p-value of the quadratic coefficient was used to test the null hypothesis that the quadratic term is equal to zero. This is equivalent to testing the Bingham residuals for a systematic quadratic pattern (Fig. 9); the residual pattern is therefore the primary evidence for non-linear flow behavior. A threshold of 0.03 was chosen instead of the conventional 0.05 to be conservative, because the equilibrium criteria defined in Section 2.3.3 only exclude steps that clearly did not stabilize. Steps that just met these criteria may still contain residual transient effects. In slightly thixotropic samples, these retained points can distort the flow curve and result in a weakly significant quadratic coefficient, i.e., apparent shear thickening, although the material is not genuinely shear thickening [63]. If the p-value was greater than 0.03, the Bingham model was retained, the quadratic coefficient was treated as zero, and the Herschel–Bulkley (Eq. 7) flow index was defined as n = 1, corresponding to Bingham-type behavior. [37]

$$\tau = \tau_0 + \mu_p \dot{\gamma} \quad (5)$$

$$\tau = \tau_0 + \mu_p \dot{\gamma} + c\dot{\gamma}^2 \quad (6)$$

$$\tau = \tau_0 + K\dot{\gamma}^n \quad (7)$$

If the p-value was below 0.03, the modified Bingham and Herschel–Bulkley models were further evaluated. In this case, the yield stress and plastic viscosity reported in the following sections are those of the modified Bingham fit. The Herschel–Bulkley flow index n was used to characterize shear-thinning or shear-thickening behavior; it quantifies the magnitude of the deviation, not its significance. For Herschel–Bulkley fitting, the Bingham yield stress and viscosity were used as starting values. If the Bingham yield stress was negative, a starting value of 0 was used instead. To improve convergence, multiple starting values for the flow index were tested: n = 0.7, 0.9, 1.0, 1.1, 1.5. The fitting constraints were: yield stress > 0, viscosity > 0 and flow index 0.5 < n < 2.3. The fit with the highest R^2 among the converged solutions was selected.

For paste, all flow-model parameters refer to the step-equilibrium points described above. For concrete, the step-down sequence could not be evaluated because a localised shear plane developed during the steps (Section 3.4); the Bingham model was therefore fitted to the ramp1down data (0.1–7.95 rpm) and the parameters are reported as apparent values, without comparison to non-linear models.

Static yield stress was determined by finding the local maximum in the smoothed data within 180–190 s (start of ramp1up).

2.4. Spread-flow measurements and flow-loss evaluation

2.4.1. Spread-flow measurements

All spread flow measurements were conducted at least twice and results were averaged. Testing was carried out under laboratory conditions at 23–25 °C. In paste, spread flow was measured based on [64]

with modifications: no compaction energy and a smooth PVC surface. The filling procedure, pre-wetting, and cone size were according to the normative procedure. Mortar spread flow measurements were according to [64] and concrete according to [65]. SP demand was considered the SP addition required to reach the target spread flow.

After the spread flow test, the sample material was poured back into the initial container and covered with a wet cloth. At the next measurement interval, the sample was stirred by hand for about 10 s in all three media, and the spread flow procedure was repeated. Boundaries for all three media are listed in Table 7, values regarding flow percentage are addressed in the next section.

2.4.2. Time of flow loss

To determine the time of flow loss, spread-flow measurements were evaluated as a function of time. For each medium, the initial target spread flow was defined as 100% flow, while a medium-specific lower limit was defined as 0% flow. The time of flow loss was then defined as the time at which the normalized flow decreased to 40% of this flow range.

For paste, mortar, and concrete, 100% flow corresponded to the measured initial spread flow of the respective mixture, which was adjusted to the target values of 260 mm, 160 mm, and 510 mm within the tolerances given in Table 7. Mixtures that did not reach the target range were excluded from this evaluation. For paste and mortar, 0% flow was defined by the bottom diameter of the flow cone. For concrete, 0% flow was defined as the lower limit of flow class F2 (350 mm) [66].

A 40% threshold was selected because spread-flow values close to the lower limit no longer represent actual flow behavior: in paste and mortar they mainly indicate limited deformation of the sample after lifting the cone rather than true spreading, and in concrete they often correspond to crumbling or local collapse within a limited diameter rather than continuous flow. The corresponding values in mm for 100, 40, and 0% flow are listed in Table 7 for the respective target spread flow; the resulting 40% threshold varies with the measured initial spread flow within the given tolerance. When the measured spread flow fell below the 40% threshold, the time of flow loss was determined by linear interpolation between the two adjacent measurement points.

3. Results and discussion

3.1. Calcined clay type controls superplasticizer demand across paste, mortar, and concrete

To evaluate the influence on rheology of calcined clay and SP type, the SP demand was compared in paste, mortar, and concrete. The demand was determined by adjusting the SP dosage required to reach the target spread flow defined for each medium (Table 7). Since the three media differ in target spread flow, calcined clay-to-solid ratio, and sample volume, absolute dosage values cannot be compared quantitatively between paste, mortar, and concrete. Therefore, the following discussion focuses on qualitative trends across media and on quantitative comparisons within each medium.

Across all investigated media, the type of calcined clay has a stronger influence on the required SP dosage than the type of SP (Fig. 3). Within one calcined clay system, the variation between different SPs tends to be comparatively small, whereas the differences between the calcined clays are much more pronounced for a given SP. This indicates that the SP demand is primarily governed by the calcined clay type.

Across the investigated media, the SP demand generally follows the order cIIlE > cIIlA > cSmI > cSmk, with the illitic calcined clays requiring the highest dosages and the smectitic calcined clay the lowest. This ranking is clearly observed in paste and mortar. In concrete, however, the ranking is modified: for SR-SP, cSmI requires a higher dosage than cIIlA. In addition, RM-SP did not achieve the target spread flow for cIIlA and cSmI within the investigated dosage range. A higher dosage did not lead to an increase in slump flow, suggesting these samples have reached their saturation limit [67]. This limitation was not apparent in paste or mortar. Moreover, cIIlE required the highest SP dosage without reaching such a saturation limit, indicating that the observed limitation was specific to certain calcined clay–SP combinations rather than being controlled by dosage level alone. These results show that the transition to concrete can both change the relative order between individual calcined clays and reveal practical limitations of specific calcined clay–SP combinations.

At the same time, the comparison between the three media shows a two-sided effect. On the one hand, the relative differences between the calcined clays become less pronounced when moving from paste to mortar and concrete. Taking cIIlE as reference within each medium, the dosage required for cSmk with SR-SP corresponds to only 15% of the cIIlE dosage in paste, 20% in mortar, and 41% in concrete. A similar tendency is observed for cIIlA and cSmI. This indicates that the calcined clay-specific contribution to SP demand is partly masked in aggregate-containing systems, where aggregate packing, paste volume, paste film thickness, and particle mobility also influence the measured spread flow [68–73]. On the other hand, the main tendencies observed in paste and mortar are still retained in concrete. In particular, cIIlE remains the most demanding calcined clay in all media, while cSmk remains among the least demanding calcined clays. This is consistent with Ferraris et al. [49], who showed that paste rheology can provide useful indications for selecting mineral admixtures such as fly ash for concrete workability. Thus, paste and mortar tests indicate transferable tendencies for SP demand, but they do not provide a quantitative prediction of concrete's SP demand for the systems investigated.

The comparatively small influence of SP type is particularly relevant considering the structural differences between the investigated PCEs. This can be seen most clearly by comparing 52HPEG6 and 52HPEG10, which have the same side-chain length but differ in backbone-to-side-chain ratio (Table 5). The higher backbone-to-side-chain ratio of 52HPEG10 results in a higher measured anionic charge compared with 52HPEG6 (3745 μeq/g vs. 2146 μeq/g). Nevertheless, this difference does not lead to a pronounced change in the required SP dosage within a given calcined clay-cement system. This is consistent with Li et al. [74], who suggested for limestone calcined clay cements (LC^3) that a higher anionic charge density can increase adsorption without necessarily improving dispersion. The comparable dosage levels obtained with SR-SP and RM-SP, despite their different chemical composition, further support that the limited influence of SP type is not restricted to the PCEs synthesized from polyethylene glycol methallyl ether macromonomers. Thus, under the investigated conditions, differences in SP type appear to play a subordinate role compared with the influence of calcined clay type. Accordingly, no clear calcined clay-specific optimum SP can be identified within the investigated set of admixtures.

Overall, the results show that SP demand is governed primarily by calcined clay type, while the investigated SPs mainly affect the exact dosage level. The high demand of cIIlE is retained from paste to concrete, identifying this calcined clay as the most critical system constituent for initial flow adjustment. Although the relative differences between calcined clays become less pronounced in aggregate-containing systems, the main tendencies observed in paste and mortar remain visible in concrete. The investigated SPs therefore allow dosage

Table 7
Boundaries for spread flow measurements, workability over time and flow loss.

medium	target spread flow	compaction energy	measurement interval	40% flow	0% flow
	mm	jolts	min	mm	mm
paste	260 ± 5	-	6, 15, 30, 45, 60, 90, 120	164	100
mortar [64]	160 ± 5	10	6, 15, 30, 45, 60, 90, 120	124	100
concrete [65]	510 ± 20	15	6, 30, 60, 90, 120	414	350

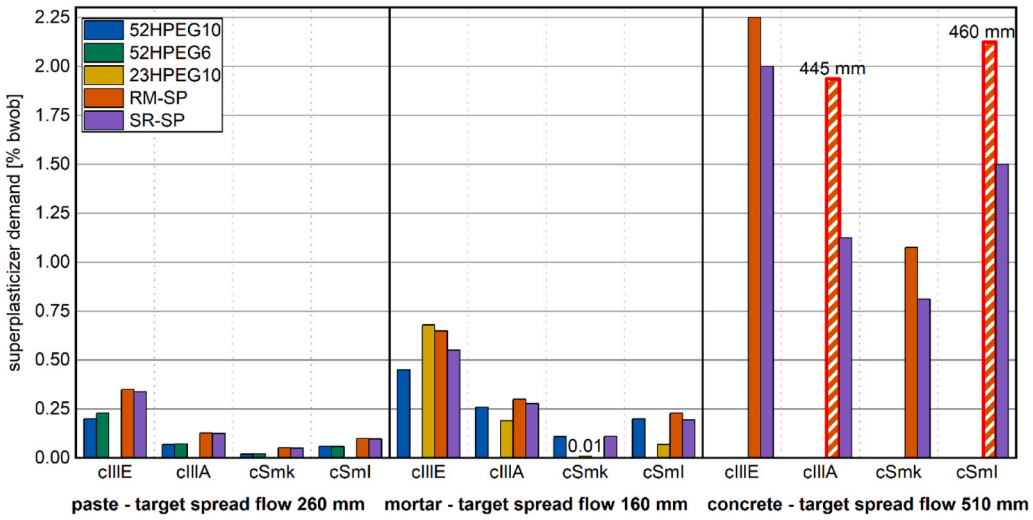


Fig. 3. SP demand in paste, mortar, and concrete. Binder composition was 70/30 vol% OPC/CC. If not specified otherwise, missing data points were not tested. Samples with hatched columns did not reach target spread flow.

adjustment within each calcined clay blended system, but they do not yet fully overcome the high demand imposed by challenging calcined clays. To understand whether this high demand originates from intrinsic rheological differences between the calcined clay cement systems, the following section first examines the early-time flow behavior of the pastes without SP and then evaluates how the efficiency of SP addition changes over time.

3.2. Calcined clay type governs flow resistance while superplasticizer efficiency declines significantly during the first 2 h

The previous section showed that using cIIIE requires the highest SP dosage to reach the target spread flow in all media and that the calcined clay-dependent demand is only partly affected by the investigated SPs. To identify the rheological origin of these differences, the early-time flow behavior of the calcined clay cement pastes was evaluated over the first 2 h. The analysis first considers the intrinsic rheological response without SP and then examines how the flow resistance reduction caused by SP addition changes with time.

3.2.1. Rheological differences between calcined clays without superplasticizer

Without SP, blended systems with the four calcined clays differ substantially in their early rheological response. Particular attention is paid to the comparison between cIIIE and cIIIA, as both calcined clays are illitic and generally similar in several material characteristics (Table 3) but led to markedly different SP demand and rheological behavior.

As summarized in Table 8, the calcined clay systems differ much more strongly in yield stress than in viscosity. The cIIIE paste shows by far the highest yield stress (81.6 Nmm). At the opposite end, cSmk paste exhibits both the lowest yield stress (21.0 Nmm) and the lowest viscosity (0.134 Nmm/rpm). Beyond these absolute levels, cSmk paste is also the only paste that approaches the transition toward shear-thickening behavior (p-value = 0.031). By contrast, viscosity remains broadly similar for all calcined clay pastes containing an illitic fraction, namely cIIIE, cIIIA, and cSmI. Since all pastes were prepared at the same solid volume fraction, viscosity is expected to be governed mainly by particle packing and by the amount of free water, whereas yield stress additionally reflects the strength of the attractive interparticle network [75]. The comparable viscosity across the illite-containing pastes therefore indicates that the calcined clays differ primarily in their colloidal interactions rather than in their volumetric packing contribution. The concurrently lower viscosity of cSmk paste is consistent with its distinctly lower BET specific surface area (37.9 m^2/g) and water adsorption capacity (50.3 wt%, compared with 65–75 wt% for the illite-containing calcined clays, Table 3). Ferrari et al. [20,21] attributed the reduced flowability of clay-containing systems to water adsorbed on the clay surface that is no longer available for flow, an effect that would be most pronounced for the samples with the highest adsorption capacity.

Table 8
Rheological parameters from rheometer measurements for 70/30 vol% OPC/CC system without SP.

Paste	yield stress	viscosity	flow resistance	p value	Hyst1	Hyst2	SBF
	Nmm	Nmm/rpm	Nmm*rpm	-	-	-	-
cIIIE	81.6	0.187	8781	0.265	0.947	0.907	1.133
cIIIA	32.4	0.179	4171	0.482	0.949	0.944	0.991
cSmk	21.0	0.134	2782	0.031	0.969	0.973	0.947
cSmI	30.8	0.186	4033	0.071	0.946	0.954	0.968

The hysteresis-based parameters reveal an additional difference. All calcined clay pastes show moderate structural breakdown within the first hysteresis loop (Ramp1). During the second hysteresis loop (Ramp2), however, a more pronounced reduction in Hyst2 is observed only for cIIIE paste (0.947–0.907), whereas the other calcined clay pastes remain comparatively stable. In combination with an SBF value greater than 1, this suggests that cIIIE paste undergoes stronger time-dependent structuration during the measurement, most likely related to ongoing hydration. This already indicates a less favorable workability retention of cIIIE paste compared to the other calcined clay pastes.

Fig. 4 further clarifies this distinction by showing the yield stress development over time without SP. In absolute terms (Fig. 4a), cIIIE paste shows the strongest increase and reaches a very high yield stress (80 Nmm) already at early age. The yield stress values of the other calcined clay pastes also increase continuously with time, but much more gradually and at substantially lower levels. Additionally, it is noteworthy that the order of yield stress values over time does not change regarding the initial order. For example, a calcined clay paste with the best initial workability also has the best workability retention, in comparison to the other investigated systems.

When the same data are normalized to the initial value at 10 min (Fig. 4b), the relative increase in yield stress appears broadly similar for all calcined clay pastes. This indicates that these calcined clay pastes

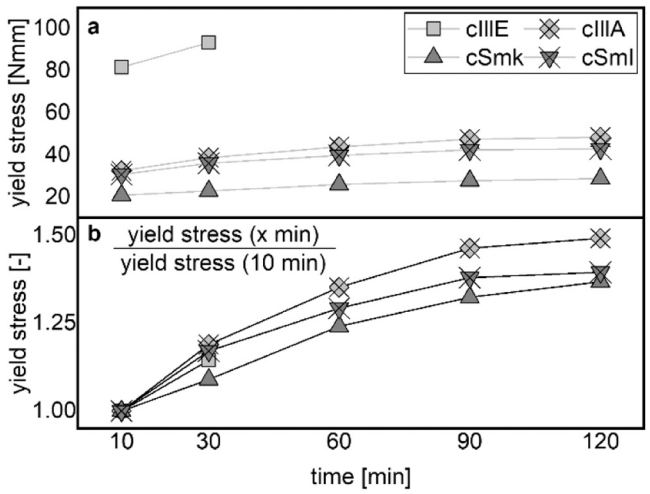


Fig. 4. Yield stress development over time for 70/30 vol% OPC/CC system without SPs. **(a)** absolute values, **(b)** relative values compared to initial yield stress at 10 min.

differ mainly in their initial yield stress, while their subsequent stiffening relative to the starting value follows a comparable trend. For cIIIE paste, a similar relative development is likely, but it cannot be assessed with certainty because the paste was no longer measurable at later times due to wall slippage.

The pronounced difference between cIIIE and cIIIA pastes therefore appears to arise primarily from the initial yield stress level. Since the two illitic calcined clays are quite similar in terms of mineralogical composition as well as several physical parameters, including BET specific surface area, water adsorption, and cation exchange capacity (Table 3), these factors cannot explain the marked rheological difference between these two calcined clay pastes. One plausible explanation is the different zeta potential of both calcined clays, which indicates different surface characteristics and affects the balance between osmotic repulsive and van der Waals attractive forces [7,30].

At the same time, pastes blended with the other calcined clays do not follow a pattern that can be explained by zeta potential alone. Additional physical parameters and particle interaction effects are therefore likely to contribute as well. Consequently, zeta potential should be regarded as a relevant, but not exclusive, parameter for explaining the observed differences in yield stress. This underlines that even calcined clays with a seemingly similar mineralogical composition cannot be treated as rheologically equivalent materials: even at 30 vol% replacement, similar calcined clays may lead to substantial differences in fresh-state behavior of the calcined clay pastes.

3.2.2. *Loss of superplasticizer efficiency over time*

After establishing the intrinsic rheological differences between pastes with different calcined clays, the effect of SP addition on the time-dependent flow resistance was evaluated using SR-SP. For this comparison, flow resistance was used instead of yield stress because several superplasticized mixtures did not provide sufficient equilibrium data points for reliable flow-curve fitting at later measurement intervals. Flow resistance allows these later measurements to be retained but may include contributions from ongoing structural breakdown and viscosity [9]. Since the extent of non-equilibrium effects may differ between samples, the discussion focuses on general time-dependent trends rather than exact absolute values.

Fig. 5a and c shows a strongly reduced initial flow resistance for all investigated calcined clay pastes due to the addition of SR-SP. When the data are normalized to the initial value at 10 min (Fig. 5b), the non-superplasticized systems show only a moderate increase in flow resistance. In contrast, the superplasticized systems (Fig. 5d) exhibit a much stronger relative increase, especially after 60 min. This increase remains partly calcined clay-dependent, with a lower relative increase for cSmk than for the illitic-containing calcined clays (cIIIA and cSmI). Thus, SP addition does not eliminate the calcined clay-specific tendency toward flow resistance build-up. Two effects may contribute to this behavior. First, the initially dispersed state can consume the available SP early [30], so that little reserve remains in the pore solution to cover the surfaces created by ongoing hydration. Second, the PCE molecular structure itself influences very early hydration kinetics: a faster ettringite formation increases the specific surface area and thereby promotes structural build-up in OPC systems [46,76]. Superplasticizer addition could therefore promote part of the structuration that its initial dispersing effect masks, which would be consistent with the stronger relative increase observed here. The interpretation for cIIIE paste is limited because measurements could not be continued after 30 min

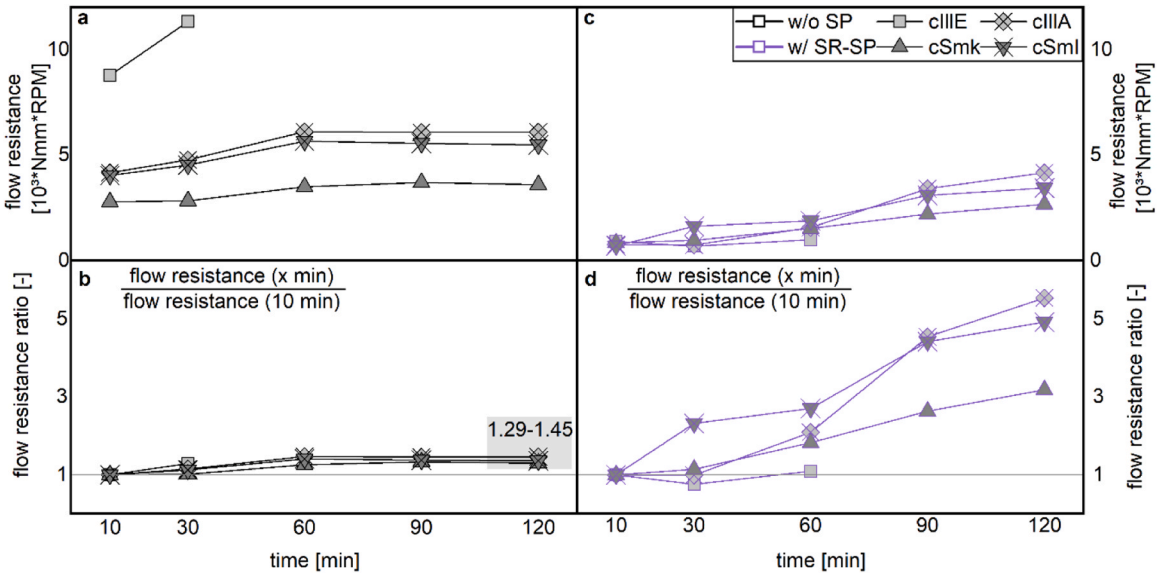


Fig. 5. Flow resistance development over time for 70/30 vol% OPC/CC paste. Absolute flow resistance over time without **(a)** and with SP **(c). Flow** resistance development over time in comparison to initial flow at 10 min without **(b)** and with SP **(d)**. Measurements for cIIIE paste without SP were not possible due to wall slippage after 30 min (60 min with SP). SP dosages according to Fig. 3.

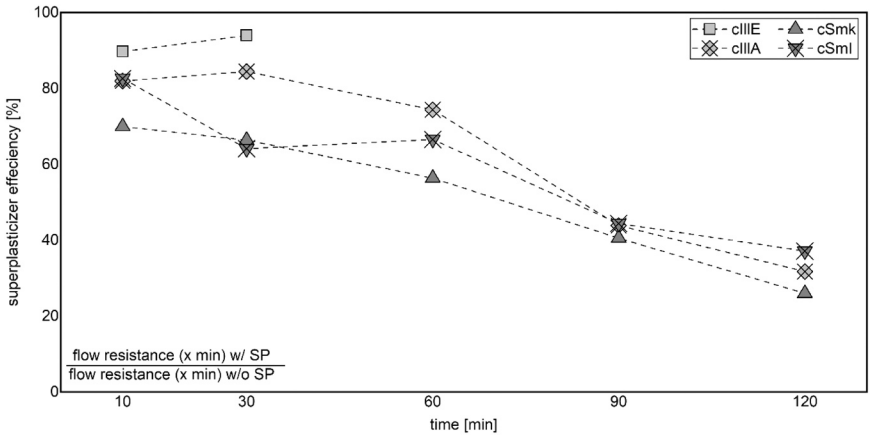


Fig. 6. SP efficiency for 70/30 vol% OPC/CC system showing the reduced flow resistance of superplasticized (SR-SP) samples in comparison to mixtures without SP at the same time interval in percentage. Calculated from data displayed in Fig. 5a and c.

without SP and after 60 min with SP due to the very stiff consistency and resulting wall slippage.

The loss of SP efficiency is further illustrated in Fig. 6, where the flow resistance of the superplasticized systems is related to the corresponding non-superplasticized reference at the same time. Despite the different absolute flow resistances of the calcined clay pastes, the normalized ratios follow a similar development: SR-SP strongly reduces initial flow resistance. At 30 min, some samples show a slight improvement in flowability, as expected for the slump-retaining SP, but by 60 min the initial reduction in flow resistance decreases continuously. At 120 min, the flow resistance of the superplasticized systems reaches approximately 60–80% of the corresponding non-superplasticized references, meaning that only about 20–40% of the reduction effect of SP remains. This indicates that the time-dependent loss of SP efficiency is a general behavior rather than being restricted to one calcined clay, even though its magnitude remains partly calcined clay-dependent.

The progressive loss of the initial improvement agrees with previous reports of flow loss in calcined clay systems despite PCE addition [22]. Therefore, the dosage required to reach an initial target spread flow should not be interpreted as an indicator of workability retention. To evaluate this behavior across paste, mortar, and concrete, the time of flow loss is considered in the following section.

3.2.3. *Time of flow loss across paste, mortar, and concrete*

To complement the rheometer-based analysis, time-dependent workability was evaluated using spread-flow measurements in paste, mortar, and concrete. Since the spread flow was measured at several time intervals, the data were reduced to one characteristic value for comparison (raw data in Table S3 and individual spread-flow curves in Figure S2). For this purpose, the time of flow loss was defined as the time at which the normalized spread flow decreased to 40% of the medium-specific flow range (Section 2.4.2).

Fig. 7 shows the time of flow loss as a function of SP dosage for all investigated calcined clays, SPs, and media. The overall trend indicates that increasing SP dosage does not lead to improved workability retention. Instead, the time of flow loss tends to decrease with increasing dosage. Due to the broad range of materials and test media included in this plot, this trend should not be interpreted as a predictive relationship. Nevertheless, it highlights that the dosage required to reach the initial target spread flow is not a reliable indicator of flow retention.

The behavior in paste differs clearly from that in mortar and concrete. In paste, the data points form distinct clusters and the time of flow loss follows the same general calcined clay-dependent tendency observed for the initial SP demand, but in reverse order. The cIIIE paste shows the shortest retention, followed by cIIIA and cSmI pastes, whereas cSmk paste results in the longest time of flow loss. However, the interpretation is not unambiguous because calcined clay type and SP dosage are coupled: The calcined clays with higher intrinsic demand also require higher dosages to reach the initial target spread flow. Therefore, this data set cannot distinguish whether the shorter flow-loss time is caused primarily by the calcined clay type, by the higher SP dosage, or by the combination of both.

In mortar and concrete, the clustering observed in paste is no longer visible, consistent with the masking effect of aggregate-containing systems discussed in Section 3.1. Most mixtures reach the defined flow-loss criterion after approximately 30 min, largely independent of calcined clay type, SP type, or dosage. The main exception is the use of cSmk with RM-SP in concrete, which retains flowability for longer than 60 min. Apart from this case, neither low nor high SP dosages lead to a systematic improvement in flow-loss time. Thus, high SP dosages may be associated with reduced flow retention in paste, whereas in mortar and concrete they do not clearly worsen the behavior but also do not prevent rapid flow loss.

This is relevant because increased SP dosage is often used to compensate for poor initial workability of calcined clay systems [28] and in ordinary cement paste an increased dosage can improve workability over time [77]. While in ordinary Portland cement SPs will adsorb over time, in LC3 more SP is adsorbed initially [27]. This could be a reason for the poor workability, independent of SP dosage. Dhers et al. [78] showed that specific surface area has an inverse correlation with workability. But since the specific surface area for the calcined clays in this study differs from 35 to 70 m^2/g and time of flow loss is similar in mortar and concrete, this may not be sufficient to explain flow loss.

Overall, the time-of-flow-loss analysis revealed a discrepancy between workability retention and initial SP demand. While the initial demand exhibited transferable tendencies from paste and mortar to concrete, the time of flow loss cannot be predicted reliably from paste measurements. Paste remains sensitive to differences between calcined clay–SP combinations, whereas mortar and concrete show a compressed response, with most systems losing flowability after approximately 30 min. Consequently, this further supports the hypothesis that the dosage required to reach an initial target spread flow should not be interpreted as an indicator of workability retention. This motivates the following section, where the effect of SP dosage on rheological stability is examined in more detail for the most demanding system, cIIIE paste.

3.3. *High superplasticizer dosage reduces yield stress but reveals thixotropy, promotes shear thickening, and accelerates relative flow loss in paste*

Pastes containing calcined clays as supplementary cementitious materials require significantly higher SP dosages to achieve comparable workability. As a result, SP dosage becomes a critical parameter

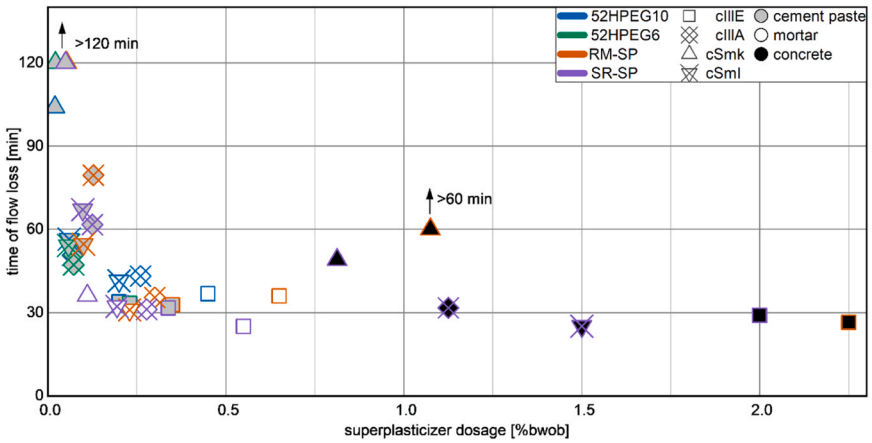


Fig. 7. Time of flow loss for different SPs and calcined clays in paste, mortar, and concrete. Binder composition was 70/30 vol% OPC/CC. SP dosage is determined by medium specific spread flow. Mixtures still above the 40% threshold at the end of testing are plotted at 120 min or 60 min and are lower bounds.

governing the rheological behavior of these systems. Therefore, this section systematically investigates the effect of one SP (52HPEG6) at different dosages in a single illitic calcined clay paste (cIIIE paste). While increasing dosage is generally intended to reduce yield stress with only minor influence on viscosity, the present results highlight that dosage also affects the time-dependent and non-linear rheological properties such as thixotropy, shear-rate-dependent viscosity, and workability retention of the system.

3.3.1. *Flow-curve analysis and transient behavior*

A first indication of dosage-dependent changes in flow behavior is given by the hysteresis loop factors Hyst1 and Hyst2 in Table 9. Hyst1 suggests an increase in thixotropy with increasing dosage. However, these parameters alone are not sufficient, as hysteresis loops cannot differentiate between thixotropy, structural breakdown, and hydration kinetics [9,73,79]. This limitation arises from the overlap of reversible and irreversible structuration mechanisms in cementitious systems, which contribute simultaneously to the measured torque response. Therefore, a more detailed analysis of the actual flow behavior is required.

Fig. 8 shows the flow curves of cIIIE paste with 52HPEG6 at stepwise increasing dosages by 0.1%bwob, together with selected sections of the flow profile smoothed and normalized for better comparison. As expected, the overall torque response decreases with increasing SP dosage. At low dosages, however, both Ramp1 (180–300 s) and Ramp2 (806–926 s) show a pronounced asymmetry between the upward and downward ramps. In particular, the plateau of Ramp2 for the sample without SP (Fig. 8d) exhibits a clear decline in torque, even though the rotational speed remains constant. Without structural effects, the torque response at constant speed would be expected to remain constant [63], as observed for dosages of 0.2%bwob and higher. The declining plateau therefore indicates ongoing destructuration under shear. Given the high shear level reached during Ramp2, this behavior is unlikely to reflect pure thixotropy, a completely time-dependent and reversible phenomenon [79]. A large part of the reversible thixotropic structure is expected to be broken down during the ramp to 100 rpm, so the continued decline in torque is more plausibly attributed to the breakdown of early hydration products. This interpretation is supported by the significantly lower (0.04) Hyst2 value compared to Hyst1 for the sample without SP. As thixotropic structuration is known to occur on short time scales (seconds to minutes) and to stabilize rapidly [80,81], a decrease in thixotropic bond strength over the investigated time interval (~10 min) is unlikely. Further evidence for hydration-driven effects is given by the plateau at Ramp2 (~115 Nmm), which is significantly higher than the torque response at 100 rpm step (103 Nmm) and ramp1 plateau, resulting in a high SBF value (Table 9). Such an increase in structural resistance over time is consistent with the progressive contribution of hydration products to the rheological response [9,81]. Accordingly, the combination of SBF $>$ 1 and Hyst2 $\ll$ Hyst1 can be interpreted as an indicator of hydration-induced structural evolution rather than purely thixotropic behavior. Under identical rest conditions, the same shear section would be expected to produce a similar response (Hyst1 =Hyst2, SBF=1) if only thixotropy were involved. The observed deviation therefore indicates that the material's microstructure changed during the interval between ramp1 and ramp2, most likely due to ongoing hydration. While the behavior at low or absent SP dosage is dominated by structural breakdown and hydration-related effects, the higher dosages increasingly reveal a distinct contribution to thixotropy. To analyze this in more detail, the transient flow behavior during changes in rotational speed is considered [9].

At 90 rpm step (Fig. 8a), all samples approach the final step response by creeping down from initially higher torque values. The inertia time

Table 9
Rheological parameters for different SP dosages for cIIIE paste in 70/30 vol% OPC/CC system with 52HPEG6.

Parameter	Unit	SP dosage in %bwob					
		0	0.1	0.2	0.3	0.4	0.5
yield stress	Nmm	81.6	48.7	34.1	25.2	17.1	9.4
Viscosity	Nmm/rpm	0.187	0.234	0.157	0.024	0.019	0.030
c	10^{-3}*Nmm/rpm^2	-	-	-	0.726	0.770	0.680
n	-	-	-	-	1.765	1.811	1.704
90 rpm transient factor	%	0.650	0.750	0.591	-0.170	0.763	-0.105
90 rpm inertia time	s	10.3	10.8	9.5	0.1	14.4	1.3
20 rpm transient factor	%	-1.857	-0.485	-0.262	-0.700	-1.227	-1.499
20 rpm recovery time	s	21.5	1.5	0.6	5.3	10.6	14.0
Hyst1	-	0.947	0.944	0.943	0.950	0.923	0.913
Hyst2	-	0.907	0.974	0.978	0.956	0.958	0.935
SBF	-	1.133	1.006	1.070	1.130	1.080	1.025

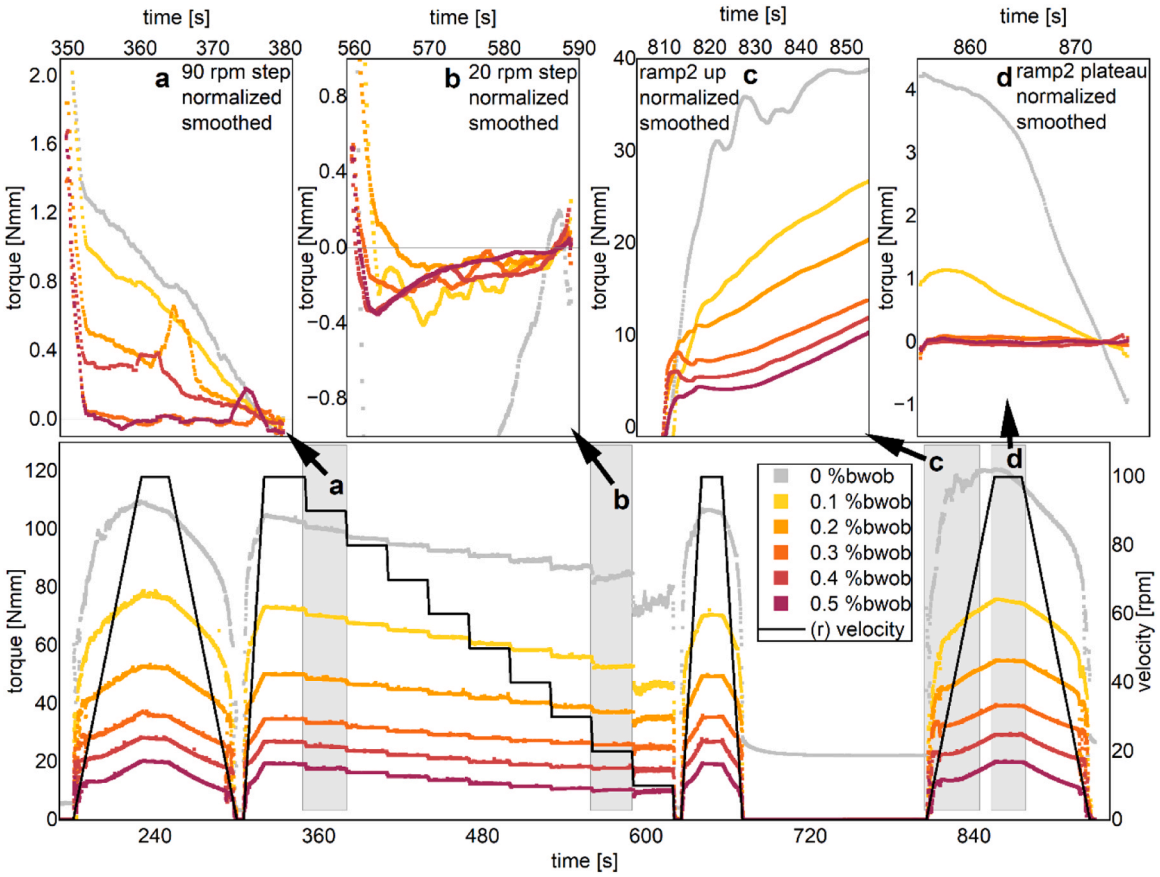


Fig. 8. Flow chart of cIllE paste with different SP dosages of 52HPEG6 for 70/30 vol% OPC/CC system. Bottom graph shows raw data points and rheometer shear profile. Top data was smoothed. **a, b** and **d** are normalized to average of the last 5 s interval of shown data points. **c** is normalized to the corresponding yield stress. The y-offset for 0%bwob observed during the rest period before ramp2 does not affect this interpretation, as repeated measurements show comparable torque values in ramp2 even in the absence of such an offset.

listed in Table 9 decreases with increasing SP dosage, with the value at 0.4%bwob excluded from interpretation due to indications of a measurement artefact in this particular step. The transient factor shows a similar trend, although the order changes slightly because it is normalized to the final mean torque of the step. For low SP dosages, the transient response is still strongly influenced by structural breakdown, and a clear distinction from thixotropy cannot be made on this basis alone.

At 20 rpm step (Fig. 8b), all samples exhibit an initial stress undershoot. While the superplasticized mixtures recover only gradually toward a constant torque response, the sample without SP shows a much stronger undershoot (partly outside the axis range) followed by a steep increase in torque, indicating rapid restructuration rather than slow equilibration. Consistently, the torque response at the plateau of Ramp2 is much higher than during the 100 rpm or during Ramp1 (Fig. 8). This suggests a significant contribution from hydration processes, which could explain the pronounced increase in torque at 20 rpm. A clear distinction between thixotropy and hydration kinetics is not possible in this sample, but a substantial hydration-related contribution appears likely.

At higher SP dosages, particularly 0.4 and 0.5%bwob, the transient response at 20 rpm showed a clearly resolved thixotropic recovery, as described by Wallevik [63]. The lower dosages (0.1, 0.2, and 0.3% bwob) also exhibit an undershoot, but the signal is more irregular and likely still affected by a competing structural process. The 20 rpm transient factor and recovery time (Table 9) both decrease up to 0.2% bwob and then increase again: from 0.3%bwob onwards, the magnitude of the transient factor roughly doubles (−0.7% to −1.5%) and the recovery time rises from 5.3 to 14.0 s, while the yield stress decreases from 25.2 to 9.4 Nmm. The thixotropic contribution thus becomes more pronounced in the step response with increasing dosage. Although these data are not precise enough to support a quantitative ranking, they clearly serve as indicative evidence for this trend.

This dosage-dependent increase in the thixotropic response appears to contrast with previous studies on OPC-based systems without calcined clays, which report a reduction in thixotropy with increasing SP adsorption or SP coverage [24,82]. However, Nicia et al. [76] also reported an increasing thixotropic structural build-up when using PCEs with short side-chains or high anionic charge density. Nevertheless, these studies investigated different SP systems and did not consider a systematic variation of dosage. Studies on kaolinitic calcined clays likewise did not vary the SP dosage: an initial increase in thixotropy with calcined clay content was reported in the absence of SP and attributed to flocculation driven by the negative surface charge and water affinity of the clay rather than to C-S-H bridging [23,40], whereas Curcio and DeAngelis [33] observed a slight reduction in thixotropy upon metakaolin addition at a fixed SP dosage and Sposito [83] reported thixotropic behavior for metamuscovite-blended pastes at a single adjusted SP dosage. In the present study, the results are based on the added dosage rather than the actual adsorption. Considering the high adsorption capacity of calcined clays, a significant portion of the SP (estimated up to ~0.8%bwob) can be bound by the calcined clay itself [30], making a complete adsorption likely.

A plausible explanation for this dosage dependence is that two contributions to the thixotropic response are superimposed. A dosage-independent contribution, referred to here as platelet-based thixotropy, is suggested by one observation and one morphological argument rather than resolved by a single measure. First, the normalized start-up response lies in a similar range across the dosage series (Fig. 8c). Second,

the platelet morphology of the calcined clays implies that randomly oriented particles have to align before steady flow is reached, a process driven by the flow itself rather than by surface forces [84] which is therefore not removed by the SP. The second contribution, referred to here as flocculation-based recovery, is attributed to the reversible re-formation of a colloidal floc network [81], consistent with the short recovery times ($\leq$ 14 s). It gains weight as the dispersed baseline decreases, and the recovery time increases because the larger relative undershoot needs longer to fall within the ±1% band (Fig. 8, Section 2.3.3). The particles thus still form a network at high SP coverage; whether PCE adsorption additionally reduces the probability of lasting contacts cannot be resolved with the present protocol. The apparent increase in thixotropy with dosage therefore reflects a reversible contribution that becomes resolvable in the step test [79] rather than a stronger structure, which resolves the apparent contrast to superplasticized OPC pastes, where the floc network is largely removed by dispersion [24,44]. The cSmk paste without SP supports this : with the lowest yield stress (21.0 Nmm, Table 8), its step response at 20 rpm (transient factor −0.56%, recovery time 2.6 s) lies between those of the illitic pastes at 0.2 and 0.3%bwob (Table 9), and thus at the transition that the illitic paste reaches only by SP addition. The governing parameter therefore appears to be the degree of flocculation rather than the SP dosage itself.

This interpretation remains to be verified, but it implies that part of the thixotropy in these pastes is revealed rather than induced by the SP, and that the morphology-related part is not reduced by a further increase in dosage. This must be taken into account when adjusting the SP dosage to the mix design.

3.3.2. *Residual analysis and emergence of shear thickening*

To quantify the deviation from linear Bingham behavior, the residuals of the Bingham fits were analyzed as a function of rotational speed (Fig. 9). For low SP dosages (0.0–0.2%bwob), the residuals provided no pronounced systematic trend, and the quadratic fit of the residuals remains statistically insignificant ($R^2 \leq 0.388$, $p \geq 0.187$). In contrast, for SP dosages of 0.3%bwob and higher, the residuals exhibit a clear and systematic curvature: the Bingham model underestimates the torque response at low and high rotational speeds and overestimates it at intermediate speeds. This produces a characteristic U-shaped residual pattern, which is well captured by a second-degree polynomial fit ($R^2 > 0.96$, $p < 10^{-4}$). A weak residual curvature is also visible at lower dosages, indicating that the Bingham model is not perfectly adequate even in these cases. However, at dosages of 0.3%bwob and higher, the pattern becomes markedly more regular and statistically significant. Notably, the most pronounced dosage-dependent change occurs at low rotational speed, particularly around 20 rpm, whereas the residuals at intermediate and high rotational speeds remain comparatively similar. This suggests that the emerging non-linearity is mainly governed by changes in the low-shear regime. The pronounced change in residuals at 20 rpm is unlikely to be a measurement artifact caused by incomplete thixotropic recovery. Fig. 8b shows that equilibrium is reached within the 20 rpm step, especially for high SP dosages. The corresponding recovery times in Table 9 are at most 14 s, which is well below the step duration of 30 s. The corresponding residual shift therefore reflects a genuine change in low-shear flow behavior.

This systematic residual structure indicates that the linear Bingham model is no longer sufficient to describe the flow behavior at higher SP dosages. Instead, the increasing positive curvature of the flow curves suggests the emergence of a shear-thickening contribution. This interpretation is consistent with earlier work by Cyr et al. [85], who explicitly investigated the conditions for the occurrence of shear thickening in pastes while varying both the type and dosage of SPs. It is also in line with more recent observations on LC3 and systems with a low water-to-cement ratio (w/c), where pastes at optimized SP dosage exhibited a transition from shear thinning to shear thickening [32,86]. A possible explanation for the similarity to low w/c systems is the high water adsorption of calcined clays, which reduces the amount of free water available for flow [20], causing these systems to behave similarly to low w/c pastes. Notably, at a fixed SP dosage, pastes containing metamuscovite showed shear thickening, whereas pastes containing metakaolin did not [42].

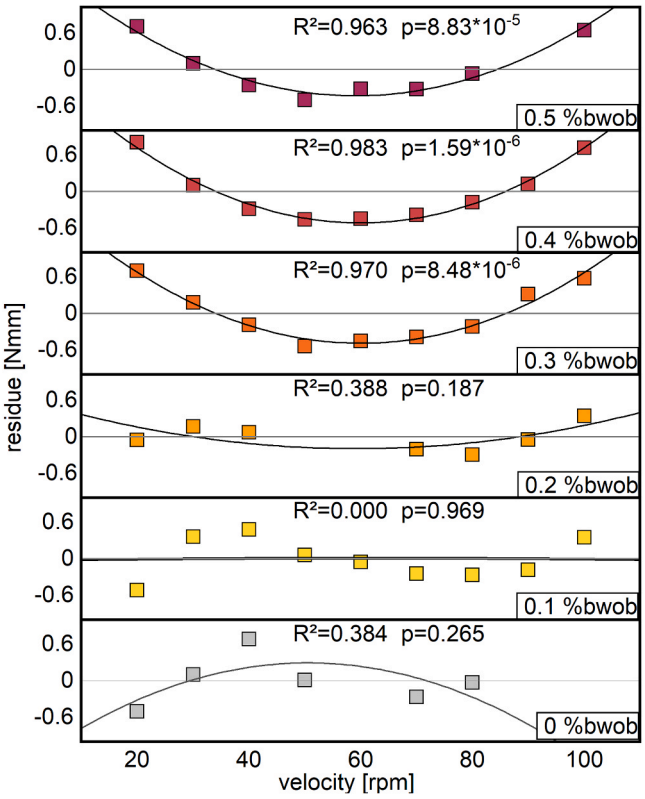


Fig. 9. Residual analysis for Bingham-fit of cIIlE paste with different SP dosages in 70/30 vol% OPC/CC system with 52HPEG6. Residuals were fitted with a second-degree polynomial to show systematic misfit. R^2 and p-value for the quadratic term are displayed. Missing values are due to lack of equilibrium conditions.

To assess whether the observed trend is limited to the cIIlE-52HPEG6 system or reflects a more general behavior, Fig. 10 compares SP dosage with two indicators of non-linear flow behavior across different calcined clays and SPs. The p-values shown in Fig. 10b indicate whether the deviation from linear Bingham behavior is statistically significant. With increasing SP dosage, p-values decrease below the chosen significance threshold of 0.03, indicating that non-linear flow behavior becomes statistically significant at higher dosage. The flow index n in Fig. 10a does not describe the significance of this deviation, but rather its magnitude. Here, a general increase in n with dosage can be observed, confirming an increasing tendency of the degree of shear-thickening behavior. Thus, although the detailed cIIlE paste analysis showed no strictly monotonic dosage-dependent increase within one individual system regarding n and c values (Table 9), the broader dataset reveals a clear overall trend: higher SP dosages promote both the occurrence and the magnitude of shear-thickening behavior across different calcined clay–SP combinations.

Although viscosity parameters obtained from Bingham, modified Bingham, and Herschel–Bulkley fits cannot be compared quantitatively, the flow-curve analysis and model evaluation indicate that the transition toward shear-thickening behavior is associated with reduced viscosity at low shear rates. This is of practical relevance for calcined clay systems, which require high superplasticizer dosages in any case (Section 3.1). Shear thickening is therefore relevant for high-shear applications such as pumping, where the required pressure rises disproportionately with discharge rate [87], which is not reflected by spread-flow tests. In

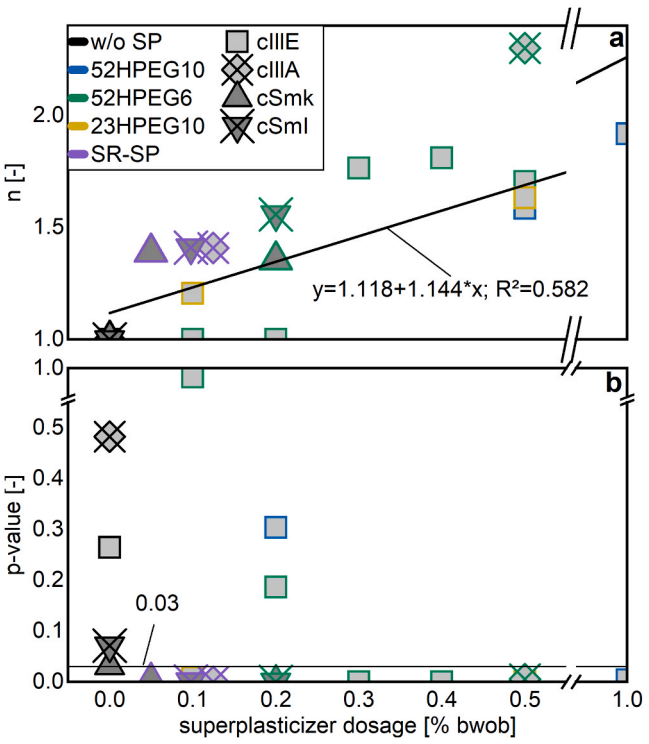


Fig. 10. Correlation of SP dosage in 70/30 vol% OPC/CC system for **(a)** flow index n and **(b)** p-value for the quadratic term of modified Bingham-Model. Including different calcined clay samples and SPs. Samples with a p-value > 0.03 have an n-value of 1 by definition (see Section 2.3.4).

addition, a sufficiently high viscosity at low shear rates is considered essential to limit segregation [88]. Since sedimentation and bleeding were not measured directly, the effect of the reduced viscosity on stability remains to be verified.

In summary, while low dosages mainly reduce yield stress as intended, higher dosages increasingly promote a shear-thickening flow response. Consequently, high dosages should be applied with caution, as they may induce non-linear shear-thickening flow behavior.

3.3.3. *Yield stress development and workability retention*

The development of yield stress was evaluated over time to further assess the practical consequences of SP dosage. Fig. 11a shows the absolute yield stress values, while Fig. 11b presents the same data normalized to the initial measurement at 10 min. As expected, increasing SP dosage strongly reduces the initial yield stress. However, the time-dependent evolution reveals a more complex correlation. The reference paste without SP and the mixtures with 0.3, 0.4, and 0.5% bwob could not be measured beyond 30 min, indicating a rapid stiffening. In contrast, the mixtures with 0.1 and 0.2%bwob remained measurable up to 120 min. It should be noted that the higher-dosage mixtures (0.3–0.5%bwob) could not be followed beyond 30 min due to loss of measurability, so their later-time evolution can only be inferred from the early increase.

The normalized data in Fig. 11b confirm that the relative increase in yield stress is not minimized by higher dosages. Rather, the 0.2%bwob mixture exhibits a faster increase (2 h, 2.7) in yield stress over time than the 0.1%bwob mixture (2 h, 2.2), despite its lower initial value. A similar tendency is already visible after 30 min. In particular, the mixtures with 0.3, 0.4, and 0.5%bwob revealed a relative increase in yield stress that is at least 50% higher than that of the reference paste without SP. This indicates an initially improved flowability at higher dosages, which may simultaneously accelerate the loss of flowability with time [22]. Consequently, the dosage that minimizes the initial yield stress is not necessarily the dosage that provides the best workability retention.

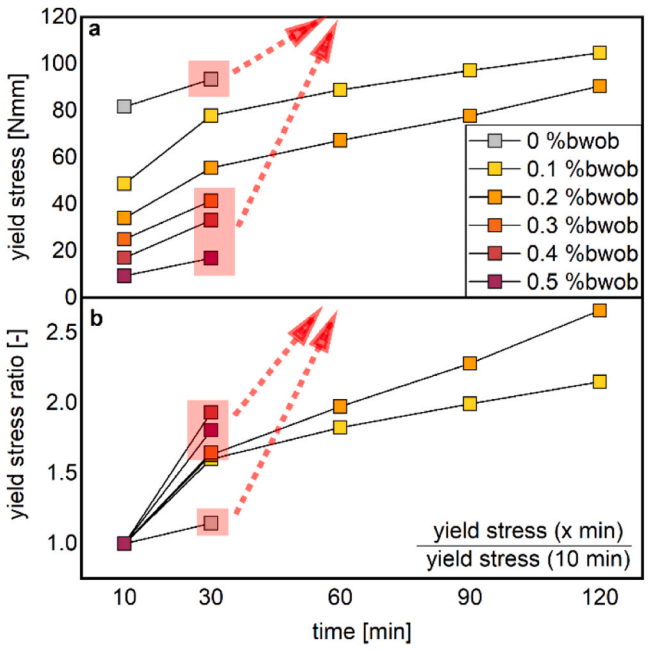


Fig. 11. Yield stress development over time for cIIIE paste with different SP dosages of 52HPEG6 in 70/30 vol% OPC/CC system. **(a)** absolute values, **(b)** relative values compared to initial yield stress at 10 min.

Flow loss in calcined clay systems is well documented even in the presence of PCE SPs [89,90], and simply increasing the dosage is not generally recommended because the improvement in workability retention is limited and segregation may become a concern. Moghul et al. [27,91] showed for superplasticized limestone calcined clay cement systems that poor workability retention remains one of the main unresolved issues and suggested that reduced effective PCE coverage on cement particles may contribute to accelerated early stiffening. This does not fully explain the results observed here, since higher dosage would be expected to increase adsorption on clinker particles and thereby extend the workability window.

One plausible explanation is a lack of reserve SP in the pore solution due to early adsorption, but it does not fully explain the accelerated time-dependent yield stress increase observed here. An additional mechanism may involve dosage-dependent changes in early hydrate structuration, especially ettringite-related structuration. Sposito et al. [22] reported that increasing phyllosilicate content and soluble aluminum ions in calcined clay systems can accelerate ettringite formation even in the presence of PCE, while large specific surface area enhances flocculation and nucleation. The ettringite formation reduces available water content with calcined clays [92].

This interpretation is supported further by literature showing that PCE interacts strongly with ettringite surfaces and that ettringite can dominate the fresh-state workability of cement suspensions [93]. In addition, SPs have been shown to influence ettringite stability and morphology, and more recent work indicates that increasing PCE dosage can alter the size and specific surface area of early ettringite even when the total amount formed changes only slightly [46].

In this context, the present results suggest that the reduced workability retention at higher dosage may not be caused solely by the absence of free SP, but also by a dosage-dependent modification of early hydrate structuration. This may explain why the mechanism proposed by [27], based on the available free cement surface, does not fully capture the behavior observed here, where increasing dosage still coincides with faster relative stiffening.

Taken together, the results show that increasing SP dosage in the present illitic calcined clay system does not simply improve workability (Fig. 12). While higher dosages strongly reduce the initial yield stress,

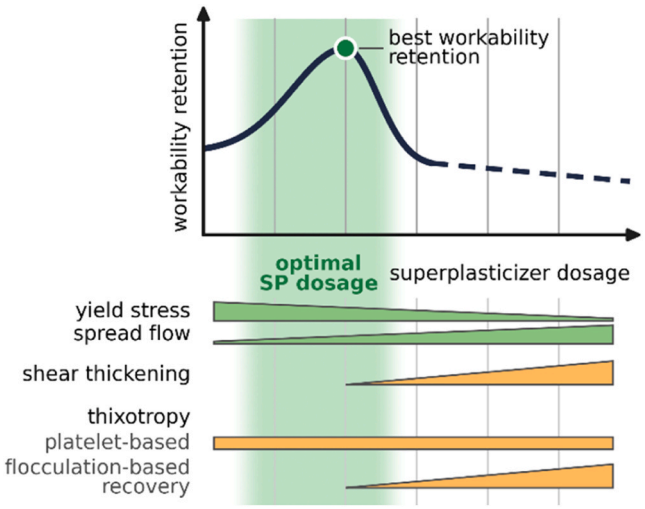


Fig. 12. Schematic illustration for optimal SP dosage in paste with partial substitution of illitic calcined clays.

they are also accompanied by an increasingly dominant flocculation-based recovery, the emergence of shear-thickening flow behavior, and a faster relative stiffening over time, whereas the hypothesized platelet-based thixotropy is not expected to depend on the dosage. Consequently, the dosage that minimizes the initial yield stress is not identical to the dosage that provides the most robust rheological performance. For the present system, moderate dosages therefore appear more favorable than high dosages when both initial workability and workability retention are considered.

3.4. Concrete flow behavior is governed by static yield stress and shear-history effects

Concrete rheometer measurements were considerably more challenging than paste measurements, since reliable measurements with the Viskomat XL require concrete mixtures to be in a sufficiently flowable state, typically F4 or higher (> 490 mm) [65]. Therefore, only mixtures that could be adjusted to high initial flowability were accessible for rheological testing. This required comparatively high SP dosages, especially for calcined clay concretes with high initial SP demand. For several calcined clay–SP combinations, however, increasing the dosage did not further improve flowability, as discussed in Section 3.1. As a result, mixtures without SP could not be evaluated reliably, nor could mixtures below the required flowability range. Time-dependent measurements were also not possible, because the samples stiffened rapidly and moved outside the reliable measurement window after the initial measurement (Fig. 7). The concrete rheometer results are therefore restricted to selected initially flowable mixtures and should be regarded as indicative rather than as a complete quantitative rheological characterization.

Compared with paste measurements, the torque response in concrete showed substantially higher scatter, which can be attributed to coarse aggregate interactions. Furthermore, in vane-type geometries, a localized shear plane may develop outside the rotating tool after a certain degree of deformation. In this case, the measured torque does not necessarily represent homogeneous deformation of the entire concrete volume. Since this behavior was partially observed during the step-down sequence, the downward steps were deemed unsuitable for a comparable evaluation. The analysis was therefore restricted to the earlier parts of the shear profile, namely the pre-shear phase and ramp1. Rheological parameters derived from a ramp are particularly sensitive to structural breakdown during the ramp. Such pronounced structural breakdown was observed for all tested concrete mixtures (Fig. 13), as indicated by the high torque response during pre-shear and the subsequent reduction (~50%) during ramp1up. Consequently, viscosity and possible apparent shear-thickening behavior may be overestimated. For this reason, the evaluation was restricted to apparent Bingham parameters from ramp1down (Section 2.3.4), and no comparison of alternative flow models was conducted.

Despite these limitations, the concrete rheometer measurements reveal several qualitative trends. First, the apparent dynamic yield stresses calculated from ramp1down are very low, with values of 32 Nmm or lower for all evaluated mixtures (Table 10). These values cannot be compared directly with paste yield stresses due to the different rheometer geometry and measurement boundaries. Nevertheless, concrete values were expected to be much higher than paste values, as aggregates are known to increase torque in general [68]. This increase can be seen for viscosity, but not for dynamic yield stress. The low dynamic yield stresses therefore suggest that the concrete was already strongly destructured by the time ramp1down was reached. This interpretation is supported by the much higher static yield stresses, which range from 122 to 262 Nmm and are much higher than the dynamic yield stresses,

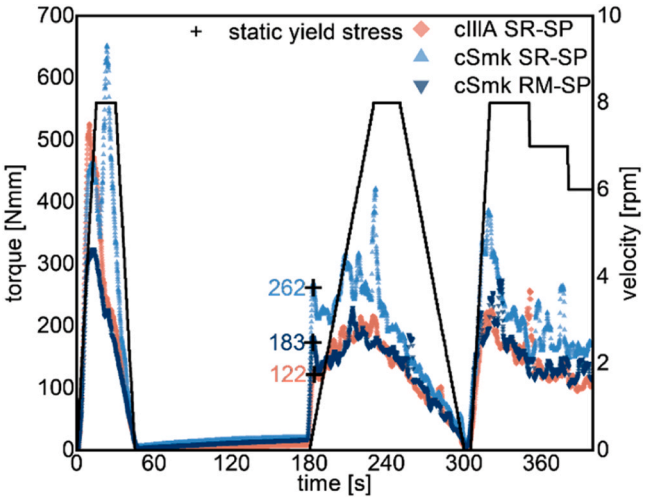


Fig. 13. Concrete rheometer smoothed torque response for selected 70/30 vol % OPC/CC concrete mixtures of pre-shear phase, ramp1 and beginning of step profile. Static yield stress was determined as the maximum of the smoothed torque signal. SP dosage was according to Fig. 3.

Table 10
Rheological parameters of concrete rheometer measurements. Yield stress and viscosity are calculated from a Bingham fit to ramp1down (Section 2.3.4). SP dosage is according to Fig. 3.

concrete	yield stress (ramp1down)	static yield stress	dynamic/static yield stress ratio	viscosity (ramp1down)	integral (ramp1up)	integral (ramp1down = flow resistance)	Hyst1
	Nmm	Nmm	%	Nmm/rpm	Nmm*rpm	Nmm*rpm	-
cIllA SR-SP	24.1	122	20	13.84	1228	619	0.504
cSmk SR-SP	32.0	262	12	17.87	1942	802	0.413
cSmk RM-SP	12.5	183	7	18.02	1255	711	0.566

resulting in dynamic/static yield-stress ratios of only 7–20% (Table 10). In paste, by contrast, static and dynamic yield stress are of similar magnitude (Fig. 8, bottom). Colloid interactions and therefore SPs are known to interact with thixotropy. Some studies report [24,44,82] reduced thixotropy due to larger interparticle distance and therefore reduced van der Waals forces. Other research observed an increased thixotropy for SPs with high anionic charge ratio and, subsequently, increased static yield stress [47]. High static yield stress in calcined clay systems may result from the combination of high SP demand and the strong influence of calcined clays on colloidal interactions [23,30]. Consequently, the high initial torque during pre-shear and the significantly lower torque during ramp1down indicate a pronounced dependence on shear history [94]. The renewed torque maximum after the short 5 s rest period following ramp1 further suggests rapid rebuilding of static yield stress. On the one hand, static yield stress is an indicator of thixotropy, on the other hand it plays a key role in resistance to segregation [9], which may partly compensate the reduced viscosity at low shear rates observed in paste (Section 3.3.2). The flow behavior of the concretes studied does not appear to be governed solely by the apparent dynamic yield stress, but rather by the balance between structural breakdown under shear and rapid recovery of static yield stress at rest.

Among the tested mixtures, cSmk concrete with SR-SP shows the highest static yield stress, although cSmk was among the least demanding calcined clays in the paste and spread-flow investigations. This inversion is not necessarily contradictory, since the two parameters describe different states [10,81]: superplasticizer demand reflects the dispersion required to reach a target flow under shear correlating to the dynamic yield stress [95], whereas static yield stress characterizes the structure rebuilt at rest. Two explanations can be considered. First, the low superplasticizer dosage required for cSmk implies a correspondingly low surface coverage, so that particles can approach each other more closely at rest and interparticle attraction increases [24]. This would raise the static yield stress without necessarily increasing the dynamic yield stress measured under shear. Second, a superplasticizer-specific effect has to be considered, since PCEs with a high anionic charge ratio have been reported to promote thixotropic structuration [76] and thereby increase static yield stress. The comparison between cSmk concrete with SR-SP and RM-SP is consistent with both explanations and indicates a strong effect of the SP type on the concrete response [47]: with SR-SP, the static yield stress is about 80 Nmm higher than with RM-SP, even though the SR-SP dosage was lower (0.81%bwob for SR-SP vs. 1.08%bwob for RM-SP). The two explanations imply opposite dosage dependencies, between which the paste results cannot distinguish (Section 3.3). Since no characteristics of the two industrial PCEs were disclosed by the supplier (Section 2.1.2), their relative contribution cannot be resolved for the present system. Although the concrete data set is limited and the observed trends should be confirmed by further investigations, the results provide useful insight into the governing mechanisms. Overall, the concrete measurements indicate that flow behavior of calcined clay containing binders in concrete is governed not only by calcined clay type, but also by shear history, static yield stress, and the specific calcined clay–SP combination.

4. Conclusion

This study investigated the influence of 2:1 phyllosilicate-dominated calcined clay types, superplasticizer type, and superplasticizer dosage on the early (2 h) flow behavior of 70/30 vol% OPC/CC systems in paste, mortar, and concrete using spread flow and rheometer measurements.

- Superplasticizer demand is governed by the calcined clay type, not by the superplasticizer used, and its general ranking (illite > smectite/illite mixture > smectite) largely transfers from paste to concrete; high dosages were required in all systems.
- Yield stress differences between the calcined clays at constant solid volume fraction originated from colloidal interactions, for which zeta potential is a relevant but not exclusive parameter. Seemingly similar calcined clays can therefore behave substantially differently in cementitious systems.
- In paste, workability retention deteriorated with superplasticizer use itself: 60–80% of the initial flow-resistance reduction dissipated within 2 h, and superplasticized pastes stiffened relatively faster than their superplasticizer-free references. These retention differences did not transfer to mortar and concrete, where most mixtures lost flowability after ~30 min regardless of clay type, superplasticizer, or dosage.
- With increasing superplasticizer dosage, the pastes transitioned from Bingham-type to non-linear flow: at ≥ 0.3%bwob, statistically significant shear thickening was observed in the residual analysis of the step-equilibrium data.
- Based on the transient analysis of the step responses, the flocculation-based recovery remained of similar absolute magnitude but became increasingly dominant as the yield stress decreased, which lengthened the recovery time. The superplasticizer thus reveals rather than induces thixotropy. A dosage-independent, platelet-based contribution was suggested but could not be verified within the present protocol.
- The dosage providing the highest initial flowability did not provide the most stable rheological performance: high dosages accelerated the relative yield-stress increase and impaired workability retention. For calcined clay systems, moderate superplasticizer dosages therefore may offer the better balance between initial workability, retention, and linear flow behavior.
- In concrete, flow behavior was governed by static yield stress and shear history: dynamic values reached only 7–20% of the static level, reflecting rapid structural rebuilding at rest. The smectitic calcined clay — despite the lowest superplasticizer demand in paste — showed the highest static yield stress in concrete and a pronounced superplasticizer-type dependency, and some clay–superplasticizer combinations proved incompatible, with flow remaining unresponsive to further dosage increases.

Future research should address the effect of high superplasticizer dosages on non-linear flow behavior and distinguish whether the rapid flow loss originates from superplasticizer adsorption on the calcined clay or from an accelerated early hydration of the system.

CRediT authorship contribution statement

Axel Neißer-Deiters: Writing – original draft, Visualization, Methodology, Investigation, Formal analysis, Data curation. **Sebastian Scherb:** Writing – review & editing, Investigation. **Nancy Beuntner:** Writing – review & editing, Funding acquisition. **Karl-Christian Thienel:** Writing – review & editing, Supervision, Funding acquisition.

Declaration of Generative AI and AI-assisted technologies in the writing process

RStudio 2026.04.0 evaluation script used for rheometer analysis was written by the authors with AI-assisted code support (OpenAI ChatGPT, various model versions between 2023 and 2026). The authors further used Anthropic Claude in order to improve the readability and language of the manuscript, and to arrange the layout and file structure of the supplementary material and the deposited dataset. After using these tools, the authors reviewed and edited the content as needed and take full responsibility for the content of the publication.

Funding

This work was supported by the Deutsche Forschungsgemeinschaft (DFG) under grant number 314833927.

Declaration of Competing Interest

The authors declare that they have no known competing financial interests or personal relationships that could have appeared to influence the work reported in this paper.

Acknowledgements

The authors thank the research group led by Prof. Plank, Professorship for Construction Chemicals, at Technical University of Munich for synthesizing and characterizing the superplasticizers.

Appendix A. Supporting information

Supplementary data associated with this article can be found in the online version at doi:10.1016/j.conbuildmat.2026.148592.

Data availability

The processed data supporting the findings of this study are provided in the supplementary material. The raw and evaluated rheometer data and the R code used for their evaluation are openly available in Mendeley Data at https://doi.org/10.17632/r87w2tkzn5.1.

References

[1] K. Scrivener, F. Martirena, S. Bishnoi, S. Maity, Calcined clay limestone cements (LC^3), Cem. Concr. Res. 114 (2018) 49–56, https://doi.org/10.1016/j.cemconres.2017.08.017.
[2] K. Scrivener, M. Sharma, F. Zunino (Eds.), Calcined Clays for Sustainable Concrete: Proceedings of the International Conference on Calcined Clays for Sustainable Concrete 2022, Springer Nature Switzerland, Cham, 2025, https://doi.org/10.1007/978-3-031-83889-7.
[3] M. Maier, N. Beuntner, K.-C. Thienel, Mineralogical characterization and reactivity test of common clays suitable as supplementary cementitious material, Appl. Clay Sci. 202 (2021) 105990, https://doi.org/10.1016/j.clay.2021.105990.
[4] A.Alujas Diaz, R.S.Almenares Reyes, T. Hanein, E.F. Irassar, M. Juenger, F. Kanavaris, M. Maier, A.T.M. Marsh, T. Sui, K.-C. Thienel, L. Valentini, B. Wang, F. Zunino, R. Snellings, Properties and occurrence of clay resources for use as supplementary cementitious materials: a paper of RILEM TC 282-CCL, Mater. Struct. 55 (2022) 139, https://doi.org/10.1617/s11527-022-01972-2.
[5] L. Ruckes, M. Maier, A. Machner, Parameters affecting the pozzolanic reactivity of common clays after mechanochemical activation, Appl. Clay Sci. 283 (2026) 108111, https://doi.org/10.1016/j.clay.2025.108111.
[6] M. Schmid, R. Sposito, K.-C. Thienel, J. Plank, The shear-thickening effect of meta muscovite as SCM and its influence on the rheological properties of ecologically optimized cementitious systems, in: V. Mechtcherine (Ed.), 2nd Int. RILEM Conf. Rheol. Process. Constr. Mater. RheoCon2, Springer, Dresden, Germany, 2019.
[7] R. Sposito, N. Beuntner, K.-C. Thienel, Characteristics of components in calcined clays and their influence on the efficiency of superplasticizers, Cem. Concr. Compos. 110 (2020), https://doi.org/10.1016/j.cemconcomp.2020.103594.
[8] N. Roussel (Ed.), Understanding the Rheology of Concrete, Woodhead Publishing, Cambridge Philadelphia, PA, 2012.
[9] M. Sonebi, D. Feys (Eds.), Measuring Rheological Properties of Cement-based Materials: State-of-the-Art Report of the RILEM Technical Committee 266-MRP, Springer Nature Switzerland, Cham, 2024, https://doi.org/10.1007/978-3-031-36743-4.
[10] M. Hayek, Y. El Bitouri, K. Bouarab, A. Yahia, Structural Build-Up of Cement Pastes: A Comprehensive Overview and Key Research Directions, Constr. Mater. 5 (2025), https://doi.org/10.3390/constrmater5020031.
[11] D. Lowke, Sedimentationsverhalten und Robustheit Selbstverdichtender Betone: Optimierung auf Basis der Modellierung der interpartikulären Wechselwirkungen in zementbasierten Suspensionen, Technische Universität München, 2013.
[12] J. Wallevik, Microstructure-Rheology: thixotropy and workability loss, Nord. Concr. Res. (2004).
[13] N. Roussel, A thixotropy model for fresh fluid concretes: Theory, validation and applications, Cem. Concr. Res. 36 (2006) 1797–1806, https://doi.org/10.1016/j.cemconres.2006.05.025.
[14] J. Mewis, N.J. Wagner, Thixotropy, Colloids Polym. Surfactants Spec. Issue Honour. Brian Vincent. 147–148 (2009) 214–227, https://doi.org/10.1016/j.cis.2008.09.005.
[15] F. Zunino, K. Scrivener, The influence of the filler effect on the sulfate requirement of blended cements, Cem. Concr. Res. 126 (2019) 105918, https://doi.org/10.1016/j.cemconres.2019.105918.
[16] M. Celia Magno, F. Venti, L. Bergamin, G. Gaglianone, G. Pierfranceschi, E. Romano, A comparison between Laser Granulometer and Sedigraph in grain size analysis of marine sediments, Measurement 128 (2018) 231–236, https://doi.org/10.1016/j.measurement.2018.06.055.
[17] M. Schmid, N. Miao, J. Plank, Shear-dependent rheological behavior of ecologically improved cements containing calcined clays as clinker substitute, in: V. Mechtcherine, S. Muthukrishnan, D. Mikhalev (Eds.), Opus Fluidum Futur. React. Multiscale Multiph. Constr. Mater. Rep. DFG SPP 2005 Prior. Program, Springer Nature Switzerland, Cham, 2026, pp. 129–148, https://doi.org/10.1007/978-3-032-15391-3_5.
[18] A. Neißer-Deiters, S. Scherb, N. Beuntner, K.-C. Thienel, Influence of the calcination temperature on the properties of a mica mineral as a suitability study for the use as SCM, Appl. Clay Sci. 179 (2019) 105168, https://doi.org/10.1016/j.clay.2019.105168.
[19] J. Berger, A. Mocciaro, G. Cordoba, C. Martinefsky, E.F. Irassar, N. Beuntner, S. Scherb, K.-C. Thienel, A. Tironi, Challenges and Performance of Filter Dusts as a Supplementary Cementitious Material, Materials 17 (2024) 5676, https://doi.org/10.3390/ma17225676.
[20] L. Ferrari, A. Nagmutdinova, A. Müller, N. Mikanovic, M. Ben-Haha, V. Bortolotti, E. Franzoni, Disclosing the mechanism behind rheological challenges in calcined clay-based cements, Constr. Build. Mater. 492 (2025) 142837, https://doi.org/10.1016/j.conbuildmat.2025.142837.
[21] L. Ferrari, V. Bortolotti, N. Mikanovic, M. Ben-Haha, E. Franzoni, Understanding workability of low carbon cements through advanced water detection techniques, Sci. Rep. 15 (2025) 35112, https://doi.org/10.1038/s41598-025-19203-3.
[22] R. Sposito, M. Maier, N. Beuntner, K.-C. Thienel, Evaluation of zeta potential of calcined clays and time-dependent flowability of blended cement with customized polycarboxylate-based superplasticizers, Constr. Build. Mater. 308 (2021) 125061, https://doi.org/10.1016/j.conbuildmat.2021.125061.
[23] P. Hou, T.R. Muzenda, Q. Li, H. Chen, S. Kawashima, T. Sui, H. Yong, N. Xie, X. Cheng, Mechanisms dominating thixotropy in limestone calcined clay cement (LC3), Cem. Concr. Res. 140 (2021) 106316, https://doi.org/10.1016/j.cemconres.2020.106316.
[24] D. Lowke, Thixotropy of SCC—A model describing the effect of particle packing and superplasticizer adsorption on thixotropic structural build-up of the mortar phase based on interparticle interactions, Cem. Concr. Res. 104 (2018) 94–104, https://doi.org/10.1016/j.cemconres.2017.11.004.
[25] S. Scherb, M. Maier, M. Köberl, N. Beuntner, K.-C. Thienel, Reaction kinetics during early hydration of calcined phyllosilicates in model cement systems, Cem. Concr. Res. 175 (2024) 107356, https://doi.org/10.1016/j.cemconres.2023.107356.
[26] M. Maier, S. Scherb, A. Neißer-Deiters, N. Beuntner, K.-C. Thienel, Hydration of cubic tricalcium aluminate in the presence of calcined clays, J. Am. Ceram. Soc. 104 (2021) 3619–3631, https://doi.org/10.1111/jace.17745.
[27] S. Moghul, F. Zunino, R.J. Flatt, Flow loss in superplasticized limestone calcined clay cement, J. Am. Ceram. Soc. 108 (2025) e20344, https://doi.org/10.1111/jace.20344.
[28] R. Sposito, M. Maier, N. Beuntner, K.-C. Thienel, Physical and mineralogical properties of calcined common clays as SCM and their impact on flow resistance and demand for superplasticizer, Cem. Concr. Res. 154 (2022) 106743, https://doi.org/10.1016/j.cemconres.2022.106743.
[29] C.M. Masolia, I.K. Kinoti, B. Mureti, J.K. Mwangi, J. Mutua, C.M. M'thiruaine, J. M. Marangu, Rheology of clay-based cement systems – a review, J. Sustain. Cem. -Based Mater. 14 (2025) 2271–2293, https://doi.org/10.1080/21650373.2025.2537268.
[30] A. Neißer-Deiters, S. Scherb, N. Beuntner, K.-C. Thienel, Rheology of calcined illitic and smectitic clays in cement-free aqueous solutions with a focus on ion adsorption

and superplasticizer interaction, Appl. Clay Sci. 283 (2026) 108101, https://doi.org/10.1016/j.clay.2025.108101.
[31] N. Nair, K. Mohammed Haneefa, M. Santhanam, R. Gettu, A study on fresh properties of limestone calcined clay blended cementitious systems, Constr. Build. Mater. 254 (2020) 119326, https://doi.org/10.1016/j.conbuildmat.2020.119326.
[32] R.K. Kandagaddala, S.V. Dhanapal, P. Nanthagopalan, Rheological characterization of limestone calcined clay cement pastes with various generations of superplasticizers for pumping applications, J. Build. Eng. 76 (2023) 107410, https://doi.org/10.1016/j.jobe.2023.107410.
[33] F. Curcio, B.A. DeAngelis, Dilatant behavior of superplasticized cement pastes containing metakaolin, Cem. Concr. Res. 28 (1998) 629–634, https://doi.org/10.1016/S0008-8846(98)00046-5.
[34] D. Feys, R. Verhoeven, G. De Schutter, Fresh self compacting concrete, a shear thickening material, Cem. Concr. Res. 38 (2008) 920–929, https://doi.org/10.1016/j.cemconres.2008.02.008.
[35] D. Feys, J. Wallevik, A. Yahia, K. Khayat, O. Wallevik, Extension of the Reiner–Riwlin equation to determine modified Bingham parameters measured in coaxial cylinders rheometers, Mater. Struct. 46 (2013) 289–311, https://doi.org/10.1617/s11527-012-9902-6.
[36] A. Yahia, A. Perrot, D. Feys, K.H. Khayat, M. Sonebi, S. Kawashima, W. Schimdt, Viscoelastic properties of fresh cement paste: measuring procedures and influencing parameters, RILEM Tech. Lett. 8 (2023) 23–30, https://doi.org/10.21809/rilemtechlett.2023.176.
[37] A. Yahia, K.H. Khayat, Analytical models for estimating yield stress of high-performance pseudoplastic grout, Cem. Concr. Res. 31 (2001) 731–738, https://doi.org/10.1016/S0008-8846(01)00476-8.
[38] R.S. Campos, G.F. Maciel, Test protocol and rheological model influence on determining the rheological properties of cement pastes, J. Build. Eng. 44 (2021) 103206, https://doi.org/10.1016/j.jobe.2021.103206.
[39] H. Ez-zaki, J. Marangu, M. Bellotto, M. Dalconi, G. Artioli, L. Valentini, A fresh view on limestone calcined clay cement (LC3) pastes, Materials 14 (2021) 3037, https://doi.org/10.3390/ma14113037.
[40] T.R. Muzenda, P. Hou, S. Kawashima, T. Sui, X. Cheng, The role of limestone and calcined clay on the rheological properties of LC3, Cem. Concr. Compos. 107 (2020) 103516, https://doi.org/10.1016/j.cemconcomp.2020.103516.
[41] S. Ferreiro, D. Herfort, J.S. Damtoft, Influence of Clay Type on Performance of Calcined Clay – Limestone Portland Cements, in: F. Martirena, A. Favier, K. Scrivener (Eds.), Calcined Clays Sustain. Concr. - Proc. 2supndsup Int. Conf. Calcined Clays Sustain. Concr., Springer, Dordrecht, Netherlands, 2017, pp. 176–182.
[42] R. Sposito, N. Beuntner, K.-C. Thienel, Rheology, setting and hydration of calcined clay blended cements in interaction with PCE-based superplasticisers, Mag. Concr. Res. 73 (2021) 785–797, https://doi.org/10.1680/jmacr.19.00488.
[43] S. Moghul, L. Köller, S. Sha, F. Zunino, R.J. Flatt, Revealing the fate of superplasticizers in blended cements, Cem. Concr. Res. 208 (2026) 108298, https://doi.org/10.1016/j.cemconres.2026.108298.
[44] Y. Qian, G. De Schutter, Different Effects of NSF and PCE Superplasticizer on Adsorption, Dynamic Yield Stress and Thixotropy of Cement Pastes, Materials 11 (2018) 695, https://doi.org/10.3390/ma11050695.
[45] K. Zhang, A. Mezhov, W. Schmidt, Chemical and thixotropic contribution to the structural build-up of cementitious materials, Constr. Build. Mater. 345 (2022) 128307, https://doi.org/10.1016/j.conbuildmat.2022.128307.
[46] O. Rindle, F. Sixt, L. Spillane, E. Willinger, T. Gädt, Revealing the morphology of nano-ettringite in cement paste: A TEM study on the influence of polycarboxylate ether superplasticizers, Cem. Concr. Res. 193 (2025) 107853, https://doi.org/10.1016/j.cemconres.2025.107853.
[47] D. Nicia, J.V. Rudolph, N. Fobbe, J. Schreiber, D. Jansen, D. Lowke, Rheology of Low Clinker Concretes with Tailored Superplasticiser Polymers: Control and Modelling of Viscosity and Thixotropic Structural Build-up, in: V. Mechtcherine, S. Muthukrishnan, D. Mikhalev (Eds.), Opus Fluidum Futur. React. Multiscale Multiph. Constr. Mater. Rep. DFG SPP 2005 Prior. Program, Springer Nature Switzerland, Cham, 2026, pp. 149–178, https://doi.org/10.1007/978-3-032-15391-3_6.
[48] J.E. Wallevik, Fresh Concrete, Mortar and Cement Paste with Various Types of Lignosulfonates, Doctoral thesis, NTNU Trondheim, Rheol. Part. Suspens. (2003).
[49] C.F. Ferraris, K.H. Obla, R. Hill, The influence of mineral admixtures on the rheology of cement paste and concrete, Cem. Concr. Res. 31 (2001) 245–255, https://doi.org/10.1016/S0008-8846(00)00454-3.
[50] DIN EN 196-3, Prüfverfahren für Zement - Teil 3: Bestimmung der Erstarrungszeiten und der Raumbeständigkeit (Methods of testing cement - Part 3: Determination of setting times and soundness), Beuth-Verlag, Berlin, Germany, 2017.
[51] DIN EN 196-1, Prüfverfahren für Zement - Teil 1: Bestimmung der Festigkeit (Methods of testing cement - Part 1: Determination of strength), Beuth-Verlag, Berlin, Germany, 2016.
[52] DIN EN ISO 17892-3, Geotechnical investigation and testing - Laboratory testing of soil - Part 3: Determination of particle density, Beuth-Verlag, Berlin, Germany, 2015.
[53] DIN EN 196-6, 2019Prüfverfahren für Zement - Teil 6: Bestimmung der Mahlfeinheit (Methods of testing cement - Part 6: Determination of fineness), Beuth Verlag, Berlin, Germany.
[54] ISO 13320, Particle size analysis - Laser diffraction methods, 2020.
[55] DIN ISO 9277, Determination of the specific surface area of solids by gas adsorption - BET method, (2014). https://doi.org/10.31030/2066286.
[56] W. Puntke, Wasseranspruch von feinen Kornhaufwerken, Beton 52 (2002) 242–248.
[57] DIN 18132, Soil, Testing Procedures and Testing Equipment - Determination of Water Absorption, Beuth-Verlag, Berlin, Germany, 2012.
[58] A. Steudel, K. Emmerich, Strategies for the successful preparation of homoionic smectites, Appl. Clay Sci. 75–76 (2013) 13–21, https://doi.org/10.1016/j.clay.2013.03.002.
[59] A. Habbaba, J. Plank, Surface chemistry of ground granulated blast furnace slag in cement pore solution and its impact on the effectiveness of polycarboxylate superplasticizers, J. Am. Ceram. Soc. 95 (2012) 768–775, https://doi.org/10.1111/j.1551-2916.2011.04968.x.
[60] M. Schmid, J. Plank, Interaction of individual meta clays with polycarboxylate (PCE) superplasticizers in cement investigated via dispersion, zeta potential and sorption measurements, Appl. Clay Sci. 207 (2021) 106092, https://doi.org/10.1016/j.clay.2021.106092.
[61] Schleibinger Geräte Teubert und Greim GmbH, Schleibinger Viskomat NT and Viskomat XL, Buchbach, Germany, 2026. https://www.schleibinger.com/cmsimple/downloads/2024_viskomat_de_compr.pdf (accessed January 8, 2026).
[62] H. Vikan, H. Justnes, F. Winnefeld, R. Figi, Correlating cement characteristics with rheology of paste, Cem. Concr. Res. 37 (2007) 1502–1511, https://doi.org/10.1016/j.cemconres.2007.08.011.
[63] J.E. Wallevik, Rheological properties of cement paste: Thixotropic behavior and structural breakdown, Cem. Concr. Res. 39 (2009) 14–29, https://doi.org/10.1016/j.cemconres.2008.10.001.
[64] DIN EN 1015-3, Prüfverfahren für Mörtel für Mauerwerk-Teil 3: Bestimmung der Konsistenz von Frischmörtel (mit Ausbreittisch) (Methods of test for mortar for masonry - Part 3: Determination of consistence of fresh mortar (by flow table)), Beuth-Verlag, Berlin, Germany, 2007.
[65] DIN EN 12350-5, 2019, Prüfung von Frischbeton - Teil 5: Ausbreitmaß (Testing fresh concrete – Part 5: Flow table test)10.31030/3045714.
[66] DIN EN 206, Beton – Festlegung, Eigenschaften, Herstellung und Konformität (Concrete - Specification, performance, production and conformity), (2021). https://doi.org/10.31030/3198971.
[67] O. Rindle, T. Gädt, Along the S-curve – how superplasticizers affect the yield stress of cement paste. Ce/Papers 6, 2023, pp. 614–620, 10.1002/cepa.2914.
[68] P. Banfill, The rheology of fresh cement and concrete—a review. Proceedings of the 11th International Congress on the Chemistry of Cement (ICCC), 2003.
[69] A.K.H. Kwan, L.G. Li, Combined effects of water film thickness and paste film thickness on rheology of mortar, Mater. Struct. 45 (2012) 1359–1374, https://doi.org/10.1617/s11527-012-9837-y.
[70] A.K.H. Kwan, L.G. Li, Combined effects of water film, paste film and mortar film thicknesses on fresh properties of concrete, Constr. Build. Mater. 50 (2014) 598–608, https://doi.org/10.1016/j.conbuildmat.2013.10.014.
[71] J.H. Lee, J.H. Kim, J.Y. Yoon, Prediction of the yield stress of concrete considering the thickness of excess paste layer, Constr. Build. Mater. 173 (2018) 411–418, https://doi.org/10.1016/j.conbuildmat.2018.03.124.
[72] L.G. Li, A.K.H. Kwan, Concrete mix design based on water film thickness and paste film thickness, Cem. Concr. Compos. 39 (2013) 33–42, https://doi.org/10.1016/j.cemconcomp.2013.03.021.
[73] G.H. Tattersall, P.F.G. Banfill, The rheology of fresh concrete, 1983. https://trid.trb.org/View/199391 (accessed March 30, 2026).
[74] R. Li, J. Xue, X. Wan, Y. Wang, J. Bao, J. Shi, T. Sui, Influence of the anionic charge of PCE superplasticizers on the rheology of LC3 cement- a mechanistic comparison with OPC, Constr. Build. Mater. 486 (2025) 141979, https://doi.org/10.1016/j.conbuildmat.2025.141979.
[75] N. Roussel, A. Lemaître, R.J. Flatt, P. Coussot, Steady state flow of cement suspensions: A micromechanical state of the art, Cem. Concr. Res. 40 (2010) 77–84, https://doi.org/10.1016/j.cemconres.2009.08.026.
[76] D. Nicia, C. Jakob, D. Jansen, D. Ivanov, O. Mazanec, J. Dengler, J. Neubauer, D. Lowke, Thixotropy of superplasticized cement pastes – underlying mechanisms considering the polycarboxylate molecular structure, interparticle interactions and hydration kinetics, Cem. Concr. Res. 173 (2023) 107289, https://doi.org/10.1016/j.cemconres.2023.107289.
[77] Y. Zhang, X. Kong, L. Gao, J. Wang, Rheological behaviors of fresh cement pastes with polycarboxylate superplasticizer, J. Wuhan. Univ. Technol. -Mater. Sci. Ed. 31 (2016) 286–299, https://doi.org/10.1007/s11595-016-1366-z.
[78] S. Dhers, A. Müller, R. Guggenberger, D. Freimut, K.S. Weldert, B. Sachsenhauser, V. Yermakou, N. Mikanovic, P. Schwesig, On the relationship between superplasticizer demand and specific surfave area of calcined clays in LC^3 systems, Constr. Build. Mater. 441 (1) (2024), https://doi.org/10.1016/j.conbuildmat.2023.134467.
[79] H.A. Barnes, Thixotropy—a review, J. Non-Newton. Fluid. Mech. 70 (1997) 1–33, https://doi.org/10.1016/S0377-0257(97)00004-9.
[80] J. Link, T. Sowoidnich, C. Pfitzner, T. Gil-Diaz, F. Heberling, J. Lützenkirchen, T. Schäfer, H.-M. Ludwig, M. Haist, The influences of cement hydration and temperature on the thixotropy of cement paste, Materials 13 (2020) 1853, https://doi.org/10.3390/ma13081853.
[81] N. Roussel, G. Ovarlez, S. Garrault, C. Brumaud, The origins of thixotropy of fresh cement pastes, Cem. Concr. Res. 42 (2012) 148–157, https://doi.org/10.1016/j.cemconres.2011.09.004.
[82] Y. El Bitouri, N. Azéma, On the "Thixotropic" Behavior of Fresh Cement Pastes, Eng 3 (2022) 677–692.
[83] R. Sposito, Investigations on the impact of metaphyllosilicates and calcined common clays on the rheology and early hydration of cements admixed with different superplasticizer, Cummulative thesis, Universität der Bundeswehr München, 2022.

[84] S. Mueller, E. Llewellin, H. Mader, The rheology of suspensions of solid particles, Proc R Soc, Proc. R. Soc. A 466 (2009) 1201–1228, https://doi.org/10.1098/rspa.2009.0445.
[85] M. Cyr, C. Legrand, M. Mouret, Study of the shear thickening effect of superplasticizers on the rheological behaviour of cement pastes containing or not mineral additives, Cem. Concr. Res. 30 (2000) 1477–1483, https://doi.org/10.1016/S0008-8846(00)00330-6.
[86] J. Liu, K. Wang, Q. Zhang, F. Han, J. Sha, J. Liu, Influence of superplasticizer dosage on the viscosity of cement paste with low water-binder ratio, Constr. Build. Mater. 149 (2017) 359–366, https://doi.org/10.1016/j.conbuildmat.2017.05.145.
[87] D. Feys, Interactions between rheological properties and pumping of self-compacting concrete. Ph.D. thesis, Ghent University, 2009. https://link.springer.com/article/10.1617/s11527-012-9912-4 (accessed October 10, 2026).
[88] K.H. Khayat, Viscosity-enhancing admixtures for cement-based materials — an overview, Cem. Concr. Compos. 20 (1998) 171–188, https://doi.org/10.1016/S0958-9465(98)80006-1.
[89] L. Ferrari, V. Bortolotti, N. Mikanovic, M. Ben Haha, E. Franzoni, A. Tagnit-Hamou, Effect of superplasticizer on water availability and rheological properties of cement paste containing calcined clay, in: ACI SP 362 12th ACIRILEM Int. Conf. Cem. Mater. Altern. Bind. Sustain. Concr., American Concrete Institute, Farmington Hills, Michigan, USA, 2024, pp. 976–985.
[90] R. Li, L. Lei, T. Sui, J. Plank, Approaches to achieve fluidity retention in low-carbon calcined clay blended cements, J. Clean. Prod. 311 (2021) 127770, https://doi.org/10.1016/j.jclepro.2021.127770.
[91] S. Moghul, L. Köller, A. Sidos, F. Zunino, R.J. Flatt, Pore solution matching: a method to resolve superplasticizer distributions in blended cements, Cem. Concr. Res. 203 (2026) 108149, https://doi.org/10.1016/j.cemconres.2026.108149.
[92] Y. Demeusy, S. Gauffinet, C. Labbez, A. Tagnit-Hamou, Rheology and Early-Age Reactivity of Calcined Kaolinite, (2024). https://doi.org/10.14359/51741015.
[93] F. Winnefeld, A. Zingg, L. Holzer, J. Pakusch, S. Becker. Ettringite-Superplasticizer Interaction and Its Impact on the Ettringite Distribution in Cement Suspensions, 2009. Sevilla, Spain.
[94] R.D. Ferron, S. Shah, E. Fuente, C. Negro, Aggregation and breakage kinetics of fresh cement paste, Cem. Concr. Res. 50 (2013) 1–10, https://doi.org/10.1016/j.cemconres.2013.03.002.
[95] N. Roussel, P. Coussot, Fifty-cent rheometer" for yield stress measurements: From slump to spreading flow, J. Rheol. 49 (2005) 705–718, https://doi.org/10.1122/1.1879041.